THE PHYSICS OF B AND D MESONS

M.S. Witherell
Department of Physics
University of California, Santa Barbara
Santa Barbara, CA 93106 USA

October 6, 1994

Contents

1 INTRODUCTION

Heavy quark physics is an enormously broad and active area of particle physics. In these lectures, I have chosen to concentrate on the weak decays of B and D mesons, plus a short section on charm spectroscopy. The goal is to describe what we are learning about the physics of these particles, and what we need to do next. I will end with a discussion of the prospects for measuring CP violation in B decays in the near future.

The *primary goal* of studying B and D decays is to understand the weak interaction. We would like to measure CKM matrix elements accurately and work toward the complete measurement of CP violation in B decays.

The *secondary goal* is to understand the nonperturbative strong interactions of heavy hadrons, which is needed to extract the weak interaction physics. The strong interactions are also interesting in their own right, for they represent a new region in which QCD properties can be calculated, using such tools as lattice gauge techniques and Heavy Quark Effective Theory (HQET). Quantities of interest are: the decay constant f_B, which is used to interpret mixing; the form factors in semileptonic decays, which is used to extract $|V_{cb}|$ and $|V_{ub}|$; and the matrix element for penguin decays, which represent a possible complication for CP studies.

There are a few important topics concerning weak decays of heavy quarks which I will introduce before exploring specific results. Later I will discuss each of them in more detail in connection with the relevant experimental measurements. They are:

1. The Cabibbo-Kobayashi-Maskawa (CKM) matrix
2. Weak Decay Diagrams
3. Decay Constants
4. Form Factors
5. Heavy Quark Effective Theory (HQET).

1.1 CKM Matrix

The hadronic weak coupling is of the form $g\ V_{jk}$, where j is the index of the up-type quark and k is the index of the down-type quark. The matrix V_{jk} is the CKM quark mixing matrix. It has the form:

$$\begin{array}{cc} & \begin{array}{ccc} d & \quad s & \quad b \end{array} \\ \begin{array}{c} u \\ c \\ t \end{array} & \begin{pmatrix} V_{ud} & V_{us} & V_{ub} \\ V_{cd} & V_{cs} & V_{cb} \\ V_{td} & V_{ts} & V_{tb} \end{pmatrix} \end{array}$$

The CKM matrix is a complex unitary matrix. After removing arbitrary phases by redefining the quark states, the matrix has 4 independent parameters. These can be understood as three mixing angles among the three generations of quarks, plus a single phase. This phase is the only possible source for CP violation within the Standard Model.

The three generation CKM matrix is most clearly represented in the Wolfenstein parameterization, which is an expansion in ($\lambda = \sin\theta_c = 0.22$):

$$V = \begin{array}{c c} & \begin{array}{ccc} d & s & b \end{array} \\ \begin{array}{c} u \\ c \\ t \end{array} & \begin{pmatrix} 1-\lambda^2/2 & \lambda & A\lambda^3(\rho - i\eta) \\ -\lambda & 1-\lambda^2/2 & A\lambda^2 \\ A\lambda^3(1-\rho-i\eta) & -A\lambda^2 & 1 \end{pmatrix} \end{array}. \tag{1}$$

Here we have ignored terms of order λ^4.

The phases are chosen in the Wolfenstein scheme such that only the elements connecting the first and third generations have imaginary parts. The four parameters in this representation are approximately (I will discuss the errors later):

1. $\lambda = |V_{us}| = \sin\theta_c = 0.22$;
2. $A = |V_{cb}|/\lambda^2 = 0.04/0.05 \approx 0.8$;
3. $(\rho^2 + \eta^2)^{1/2} = |V_{ub}|/|V_{cb}|\lambda = 0.08/0.22 \approx 0.35$; and
4. $\eta/\rho = ?$.

There is a simple way of displaying the limits of our knowledge about the CKM matrix. If we apply the unitarity condition to the first and third columns in the CKM matrix, we get the expression:

$$V_{ud}V_{ub}^* + V_{cd}V_{cb}^* + V_{td}V_{tb}^* = 0. \tag{2}$$

which is approximately

$$V_{ub}^* + V_{td} = -V_{cd}V_{cb}^*. \tag{3}$$

This gives a triangle in the complex plane, as shown in figure 1. All CP-violating amplitudes are proportional to its area.

Most of our information on the CKM parameters comes from measurements of semileptonic decays. We use additional experimental information to complete our knowledge of the CKM matrix: the CP-violation parameter ϵ from $K_L^0 \to \pi\pi$ and the top quark mass m_t from CDF or LEP. We also need various hadronic matrix elements from theory. In section 2, I will review the experimental results from B decays that determine the CKM parameters, their interpretation, and the present status of the CKM matrix.

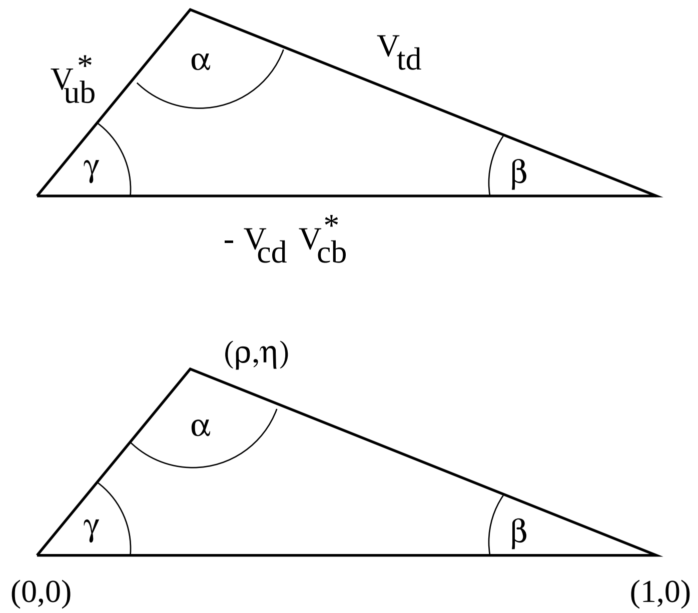

Figure 1: The unitarity triangle: (top) before and (bottom) after dividing by the length of the base. The three angles α, β, and γ determine the CP-violating asymmetries in B^0 decay.

Thirty years after the initial discovery of CP violation, we are still trying to understand its origin. What causes the fundamental asymmetry between particle and antiparticle? With the single phase in the CKM matrix, we have a natural explanation for CP violation within the Standard Model. Yet we have no convincing evidence to confirm the explanation. This brings us to the fundamental question, which experiment must answer:

1. Is CP violation intrinsic to the Standard Model?

2. Or is it the first experimental result contradicting the Standard Model?

This is the central issue which drives the field of heavy quark physics. If it is intrinsic to the Standard Model, then the SM has passed the last major test before the Higgs. We would still need to understand what causes the values of masses and CKM elements, however, which is in itself of fundamental importance. If the SM does not explain CP violation, then we have found the clue to the next level of physics. We would then need to track down the source.

As we will discuss at the end of these lectures, the signature test of the Standard Model explanation of CP violation is whether the large CP-violating asymmetries predicted from the experimental constraints on the unitarity triangle are in fact observed.

1.2 Decay Diagrams

Before discussing the physics of weak decays of heavy mesons, I introduce the various quark decay diagrams that are involved.

Spectator diagrams, such as those shown in figure 2, are those in which only the heavy quark is involved at the weak vertex. The light antiquark is a spectator, involved only in the hadronization process that produces the final-state particles. Spectator diagrams dominate the total decay rate and therefore control the B lifetimes.

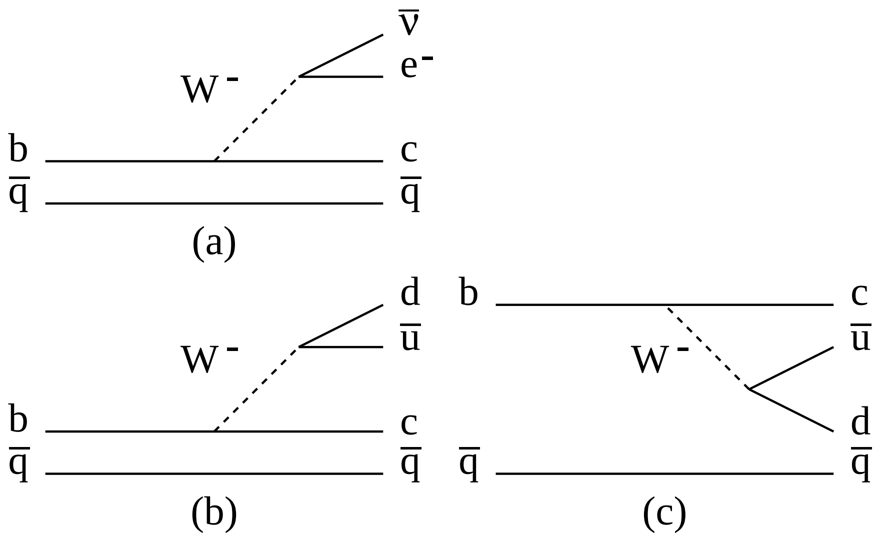

Figure 2: The spectator diagrams for B decays: (a) semileptonic, (b) external W hadronic, and (c)internal W hadronic.

In nonspectator decays, such as those shown in figure 3, both the initial-state quarks are involved in the weak vertex. The leptonic decay is familiar from the decay $\pi^+ \to \mu^+\nu$, which dominates the decay rate because the helicity suppression is not as effective as in the case of $\pi^+ \to e^+\nu$. For B mesons, all of the leptonic decays are small because of helicity suppression. The rate is proportional to the square of the lepton mass:

$$\Gamma(B^- \to \ell^- \overline{\nu}) = \frac{G^2}{8\pi} |V_{cb}|^2 f_B^2 \; m_B \; m_\ell^2 [1 - m_\ell^2/m_B^2]^2. \tag{4}$$

The largest branching ratio is $B^- \to \tau^- \overline{\nu}$, with an expected branching ratio of $\approx 10^{-4}$.

The W exchange diagram shown in figure 3 is the principal nonspectator diagram contributing to the hadronic decay rate. It only applies to B_d^0 and B_s^0 decays. Scaling from experience with charm decay, we expect the contribution from this decay to be very small compared to spectator decays.

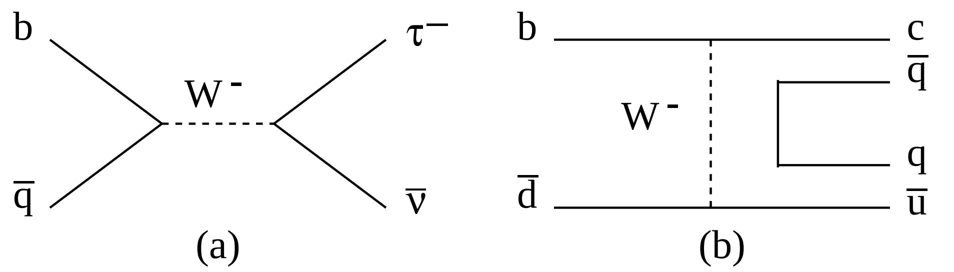

Figure 3: The nonspectator diagrams for B decays: (a) leptonic and (b) W exchange.

Penguin decays, shown in figure 4, are one-loop diagrams that result in an effective flavor-changing neutral current. The inclusive rate can be calculated reasonably well, with an uncertainty due to the error on m_t. An important part of this calculation are the QCD corrections, which are not shown in the diagram.

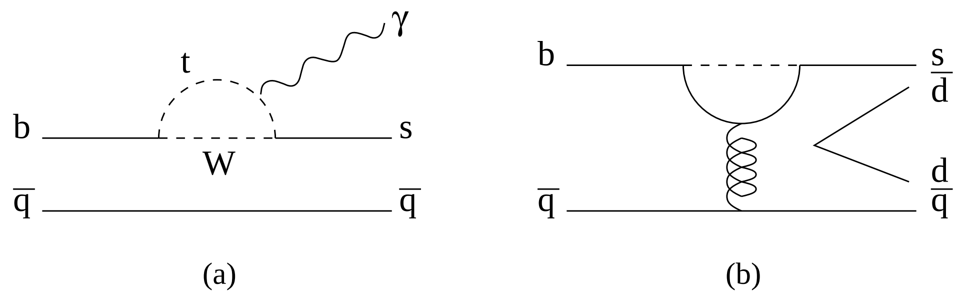

Figure 4: The penguin diagrams for B decays: (a) electromagnetic penguin and (b) hadronic penguin.

Finally, figure 5 shows the second-order weak diagrams for mixing, which is used to measure $|V_{td}|$. Interference of mixed and unmixed diagrams makes it possible to obtain measurement of the CP violation parameters in certain B^0 decays with no uncertainty due to a hadronic matrix element.

1.3 Decay Constants

The decay constant for the light mesons is traditionally measured using the purely leptonic decay, such as $\pi^+ \to \mu^+\nu$. The rate for the decay $B^- \to \ell^-\overline{\nu}$ is given in equation 1. Because the weak interaction is effectively a point interaction at low energy, the decay constant is proportional to the probability that the two quarks in the meson have zero separation. The decay constant is also involved in the amplitudes for hadronic spectator decay and

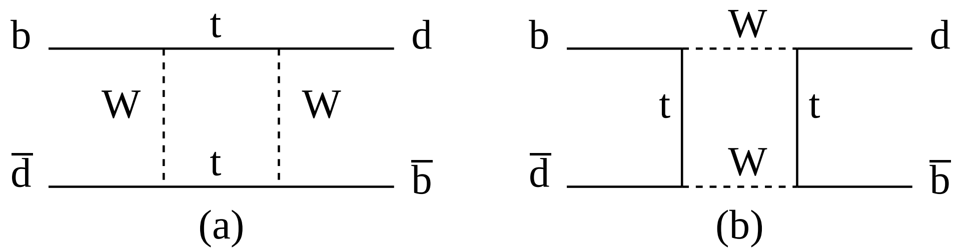

Figure 5: The mixing diagrams for $B^0 - \overline{B}^0$ mixing.

mixing. The calculation of f_B and f_D is one of the main goals for lattice gauge efforts. The main experimental test of these calculations in the near future is the D_s^+ decay constant, which has now been measured, but with large errors.

1.4 Form Factors

The diagram for semileptonic decay is shown in figure 2. The differential decay rate for $B \to D\ell\nu$ is given by

$$\frac{d\Gamma}{dq^2} = \frac{G^2}{24\pi^3} \; |V_{cs}|^2 \; P_D^3 \; f_+^2(q^2). \tag{5}$$

where $f_+(q^2)$ is the single vector form factor. Roughly speaking, $|f_+(q^2)|^2$ represents the probability that the final state quarks will form a particular meson, such as the D in this case. The form factor is highest when the final state meson is at rest in the frame of the parent meson, although the rate is suppressed there because of the P_D^3 factor. Figure 6 shows the configuration of a B before decay, and after decay for the two extreme values of q^2.

The form factor is therefore at its maximum when the final state meson is at rest in the B frame, which occurs at $q^2 = q^2_{\rm max} = (M_B - M_D)^2$. At $q^2 = q^2_{\rm min} \approx 0$, $E_D = (M_B^2 + M_D^2)/(2M_B) \approx 3$ GeV, and the form factor is at its minimum. The similar expression for $B \to D^*\ell\nu$ involves three form factors and is correspondingly more complex.

1.5 Heavy Quark Effective Theory

New insights into the behavior of hadrons containing a heavy quark and light constituents (quarks and gluons) have come from the application of Heavy Quark Effective Theory (HQET)[1]. The original flavor symmetry of the strong interactions is isospin symmetry, which is based on the fact that $m_u - m_d << \Lambda_{QCD}$. There is also a heavy quark symmetry in the limit that $m_Q >> \Lambda_{QCD}$. This symmetry is the basis for HQET. In this limit, the

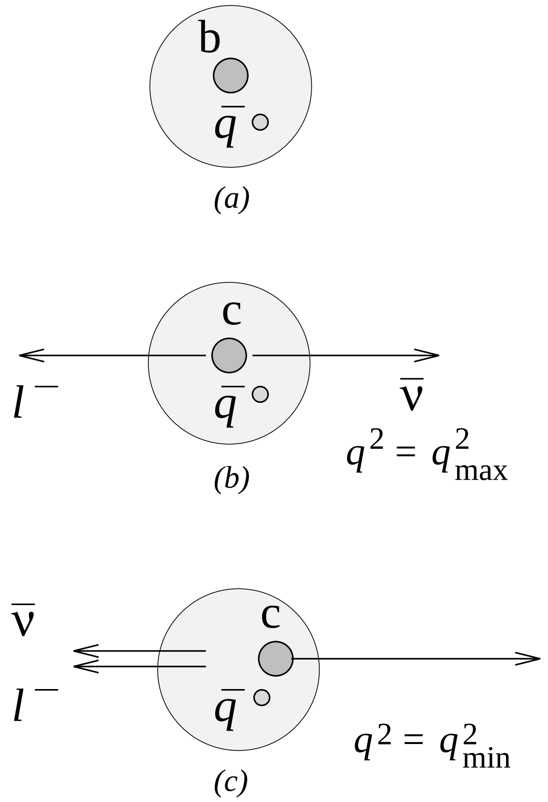

Figure 6: Kinematic configurations for the decay $B \to X_c \ell \nu$: (a) B-meson before decay; (b) decay configuration for $q^2 = q^2_{\rm max}$, and (c) configuration for $q^2 = q^2_{\rm min}$.

heavy quark is effectively a static source of a color-triplet field. The wave function of the light quark and gluons do not depend on either the mass or the spin of the heavy quark.

HQET is an expansion of QCD, and is therefore not a model. Corrections of order Λ_{QCD}/m_Q and α_S must be calculated, but it gives a systematic way of expanding the strong interactions of heavy particles, and of understanding the error of the predictions. Some of the applications of HQET are calculations of the form factors for $B \to D\ell\nu$ and $B \to D^*\ell\nu$ at zero recoil of the D or D^* meson, and predictions for the mass splittings of excited charm mesons.

2 CKM MEASUREMENTS USING B DECAYS

We measure the CKM matrix elements $|V_{cb}|$ and $|V_{ub}|$ using semileptonic decays because they are easier to interpret than hadronic decays. The leptonic current is exactly known, and the strong interaction is completely described by a form factor. The diagram for the dominant semileptonic decays, $\overline{B} \to D^{(*)}\ell\nu$ is shown in figure 7.

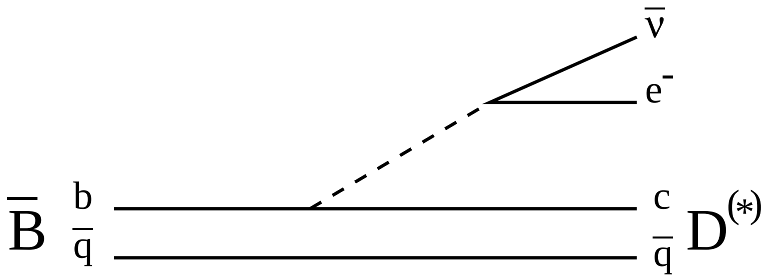

Figure 7: The quark diagram for $B \to D^{(*)}\ell\nu$.

There are four semileptonic decays of heavy quarks, at the quark level, and we learn something different from each of them.

- $c \to s(d)\ell\nu$.
    1. The CKM matrix element is known. $|V_{cs}| = 0.975$
    2. We want to measure the form factors and check the calculations.
- $b \to c\ell\nu$.
    1. The form factors are known at the zero-recoil point from HQET, including corrections.
    2. We should be able to reliably measure $|V_{cb}|$.
- $b \to u\ell\nu$.
    1. The CKM matrix element $|V_{ub}|$is not known from other sources.
    2. The form factors are not predicted well by models or HQET.

The form factors for $B \to \pi(\rho)\ell\nu$ are related to those for $D \to \pi(\rho)\ell\nu$ at high q^2 by HQET, with suitable corrections. They are further related to the much better measured form factors for $D \to K(K^*)\ell\nu$ using SU(3).

2.1 Measuring $|V_{cb}|$

$|V_{cb}|$ is measured using both inclusive and exclusive semileptonic decays. The two methods involve different experimental and theoretical complexities. The branching ratio for the inclusive decay $B \to X_c \ell \nu$ is measured rather precisely. An important issue is the reliability of the inclusive models, in particular the sensitivity to quark masses and QCD corrections. Measurements of the exclusive decay $B \to D^* \ell \nu$ are starting to become quite precise. HQET provides powerful method for determining form factors, at least near zero recoil. I will now discuss each of these methods for measuring $|V_{cb}|$ in some detail.

2.1.1 $|V_{cb}|$ from Inclusive Semileptonic Decays

At the $\Upsilon(4S)$, $B(B \to X_c \ell \nu)$ is measured by selecting events containing a lepton using minimal analysis cuts, subtracting the continuum background and other lepton sources, and fitting the lepton-energy spectrum. The difficult part is separating the contributions of primary leptons from $B \to X_c \ell \nu$ and the secondary leptons from $B \to D + X,\ D \to Y \ell \nu$. The high-statistics spectrum from CLEO [2], shown in figure 8, is fitted to the two main components using a model for the shape of the primary-lepton spectrum and measured spectra for both steps in the secondary process.

There are two models used: (a) an inclusive parton model, the ACCMM [3] model; and (b) an exclusive model, a modified version of the ISGW [4] model, usually called ISGW**. In the ACCMM model there are two parameters, the c-quark mass and the effective Fermi momentum of the spectator quark inside the meson. In the original ISGW model, the relative fractions of $D/D^*/D^{**}$ in the final state are fixed. In the ISGW** model, the amount of D^{**} is allowed to float, and in the CLEO fit [2] it takes up $(21 \pm 2 \pm 8)$ of the inclusive rate, higher than in the ISGW model. The ratio D^*/D is fixed at the value (2.3) predicted by ISGW. In this fit, the D^{**} component includes all of the $\ell = 1$ and radially excited D resonances, plus any nonresonant $B \to D\pi\ell\nu$ decay that may exist. The fits to both the ACCMM model and the modified ISGW model are quite good. The results from the CLEO analysis and a similar ARGUS analysis [5] are shown in table 1.

ARGUS [6] developed a second method to extract the inclusive semileptonic branching fraction without using a model of the spectrum. They use the charge correlation in dilepton events to separate primary from secondary leptons: As the tagging lepton, they choose a lepton with $p_\ell > 1.4$ GeV/c, a region in which virtually all leptons are primary. They then study the momentum spectrum of the second lepton in the event. If it is of charge opposite from the tagging lepton, it is probably a primary lepton, if the same then a secondary lepton. There are two sources of wrong charge correlation:

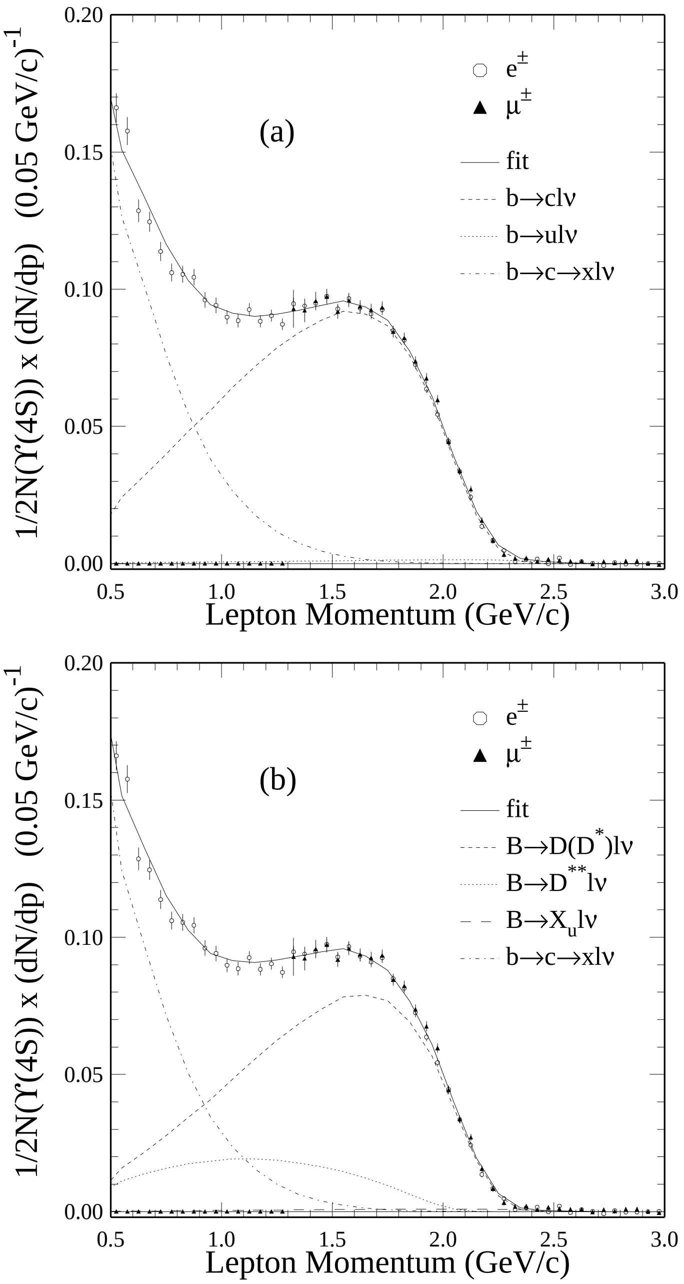

Figure 8: The inclusive lepton momentum spectrum from $B \to X\ell\nu$, with fits to (a) the ACCMM model and (b) the ISGW** model, which allows more D^{**} than in the original ISGW model.

Exp	Method/Model	$B(B \to X_c \ell \nu)\%$
CLEO[2]	1ℓ ACCMM	$10.48 \pm 0.07 \pm 0.33$
	ISGW**	$10.87 \pm 0.10 \pm 0.33$
ARGUS[5]	1ℓ ACCMM	$10.2 \pm 0.5 \pm 0.2$
ARGUS[6]	2ℓ	$9.6 \pm 0.5 \pm 0.4$
CLEO[7]	2ℓ	$10.36 \pm 0.17 \pm 0.40$
LEP Avg.[8]	$1+2\ \ell$ ACCMM	$11.0 \pm 0.3 \pm 0.4$
PDG Avg.[9]		10.4 ± 0.4

Table 1: Measurements of $B(B \to X_c \ell \nu)$ The ISGW fit is to the modified ISGW model described in the text.

(1) $B \to \ell_P^+ \, D^-, D^- \to \ell_S^-$, $B^- \to X$; and (2) $B^0 \to \overline{B}^0 \to \ell_P^-$ (mixing). The first is suppressed by requiring $\cos\theta_{\ell\ell} > 0$, which is very unlikely if they come from the same B. A correction is applied for the mixing contribution. This technique allows one to extract $\frac{dN_P}{dP_\ell}$ with only a small model dependence.

The branching ratio resulting from this method, shown in table 1, agrees with that from the single lepton method. It has poorer statistical error, but better systematic. A similar CLEO dilepton analysis with higher statistics also confirms the single-lepton result [7].

Measurements from LEP experiments [8] of the inclusive b-hadron semileptonic branching fraction include B_s and Λ_b decays. The measurements there, summarized in table 1, agree with the measurements from CLEO and ARGUS, suggesting that the lifetimes of the various hadrons are not very different. These measurements must also assume the lepton spectrum in the B center-of-mass, which is checked by the fits to the CLEO and ARGUS data.

To extract the CKM matrix element from the semileptonic branching fraction, one uses the equation:

$$B(B \to X_c \ell \nu) = \gamma_c |V_{cb}|^2 \tau_B, \tag{6}$$

where the factor γ_c comes from a decay model. The PDG average corresponds to

$$|V_{cb}| = 0.40 \pm 0.001 \pm 0.004 \tag{7}$$

assuming a lifetime of 1.54 ps. The first error is the total experimental error, and the second is the theoretical error, corresponding to a 20% error in the rate. This error is effectively due to the uncertainty in the bottom and charm quark masses, which is larger than the differences between models for given quark masses. Shifman, Uraltsev, and Vainshtein [10] argue the result is primarily sensitive to $m_b - m_c$, and that the corresponding error on $|V_{cb}|$ should be only ± 0.002.

2.1.2 $|V_{cb}|$ from Exclusive Semileptonic Decays

Two modes dominate $B \to X_c \ell \nu$ decays: $B \to D\ell\nu$ and $B \to D^* \ell \nu$. For $B \to D\ell\nu$, the rate is given by the expression in equation 5. The connection between measurement and CKM element is rather simple, but extracting $|V_{cb}|$ from this mode is experimentally difficult. In particular, it is difficult to isolate a clean sample of events. The competing decay $B \to D^*\ell\nu$, $D^* \to D\pi(\gamma)$ produces three times as many $D^0\ell$ events as does direct decay, making it very hard to use $B^- \to D^0\ell^-\nu$. And the $\overline{B}^0 \to D^{*+}\ell^-\overline{\nu}$ decays are accompanied by a large background underneath the $D^+ \to K^-\pi^+\pi^+$ peak. Finally, the decay rate is highly suppressed when the final state D meson has zero recoil momentum, which is where the form factor is best determined, as seen in equation 5.

Thus, measuring $B \to D^*\ell\nu$ is the best way to determine $|V_{cb}|$ in exclusive decays. $\overline{B}^0 \to D^{*+(0)}\ell^-\overline{\nu}$, $D^{*+(0)} \to \pi^{+(0)}D^0$ is very clean. Because the decay with $\ell = 0$ is allowed, the rate is substantial fairly near the kinematic limit of zero recoil momentum, where the form factors are predicted by HQET. The initial data sample consists of events with a $D^* \to \pi D^0$ candidate and a good lepton. One plots $M^2_{miss} = (M_B - E_{D^*\ell})^2 - P^2_{D^*\ell}$ to see if it is consistent with $M^2_\nu = 0$. The resulting CLEO [11] measurement of the branching ratio is shown in table 2.

In a second method, first employed by ARGUS [12], the D^{*+} in the $B(\overline{B}^0 \to D^{*+}\ell^-\overline{\nu})$ is identified using only the soft pion from the $D^{*+} \to \pi^+D^0$ decay (partial reconstruction). By using this technique, they get a comparable statistical error with a much smaller data sample. The result from this measurement is also shown in table 2.

Exp	$B(\overline{B}^0 \to D^{*+}\ell^-\overline{\nu})$
CLEO	$4.49 \pm 0.32 \pm 0.39$
ARGUS	$4.5 \pm 0.3 \pm 0.4$

Table 2: Measurements of the branching ratio $B(\overline{B}^0 \to D^{*+}\ell^-\overline{\nu})$. The CLEO measurement combines data from both $\overline{B}^0$ and B^- decays.

Using this branching ratio is not the best way to extract $|V_{cb}|$ from the data, however, because of model uncertainties. We would like to make use the fact that HQET can accurately predict the differential decay rate for $B \to D^*\ell\nu$ at zero recoil. At zero recoil ($q^2 = q^2_{max}$), the light objects in the meson ($\overline{q}$, gluons) are undisturbed by the $b \to c$ transition, in the limit that both heavy quarks have infinite mass.

One can relate all three $D^*\ell\overline{\nu}$ form factors to a single form factor in

HQET, the Isgur-Wise function $\xi(w)$. It is defined in terms of the variable

$$w = \frac{m_B^2 + m_{D^*}^2 - q^2}{2\, m_B m_{D^*}}, \tag{8}$$

which is just the relativistic γ of the D^* in the B rest frame. Thus the zero recoil point corresponds to $w = 1$. The HQET limit at zero recoil determines the normalization at this point: $\xi = 1.0$. There are no corrections to this limit of order $(1/m_Q)$ at w=1 [13]; the leading corrections are of order $(1/m_Q^2)$, and are somewhat model dependent. Neubert has obtained the result

$$\begin{aligned}\frac{1}{\tau_B} \cdot \frac{dB(\overline{B}^0 \to D^{*+}\ell^-\overline{\nu})}{dw} &= \frac{G_F^2}{48\pi^3} m_{D^*}^3 \left(m_B - m_{D^*}\right)^2 \sqrt{w^2-1}(w+1)^2 \times \\ & \left[1 + \frac{4w}{w+1}\frac{1-2wr+r^2}{(1-r)^2}\right] |V_{cb}|^2 F(w)^2, \end{aligned} \tag{9}$$

where $r = m_{D^*}/m_B$, and $F(1) \approx 1$. The unknown function $F(w)$ is closely related to $\xi(w)$, as discussed by Neubert [14], but includes symmetry breaking corrections. In particular, there are a number of calculations of $F(1)$: 0.96 ± 0.03 [15], 0.93 ± 0.03 [14], and 0.89 ± 0.03 [10].

Experimentally, measuring the differential decay rate at $w = 1$ is difficult because at that point the D^* is moving slowly, leading to a very slow decay pion for experiments operating at the $\Upsilon(4S)$. It is necessary to rely on an extrapolation of the measurements from higher values of w. This does not make the task impossible, however, because the range of w is small, and $F(w)$ is expected to be approximately linear. One has to be careful about understanding the dependence of the efficiency for slow charged and neutral pions on the momentum. Typically, experiments use a function of the form

$$F(w) = F(1)[1 - \hat{\rho}^2(w-1)], \tag{10}$$

although sometimes exponential or quadratic forms are used.

Exp	$\|V_{cb}\|F(1)$	$\hat{\rho}^2$
CLEO [11]	$0.0351 \pm 0.0019 \pm 0.0018 \pm 0.0008$	$0.84 \pm 0.13 \pm 0.08$
ARGUS [17]	$0.041 \pm 0.005 \pm 0.003$	$1.17 \pm 0.22 \pm 0.06$

Table 3: Measurements of $|V_{cb}|$ and $\hat{\rho}^2$ using the decay $\overline{B}^0 \to D^{*+}\ell^-\overline{\nu}$ and HQET predictions. The ARGUS result has been corrected to a B^0 lifetime of 1.54 ps.

The experiments divide out all of the kinematic factors, so that what is plotted is $|V_{cb}|F(w)$. They then fit this plot with two parameters: (a) the intercept at $w = 1$ gives $|V_{cb}|F(1)$; (b) the slope gives the size parameter

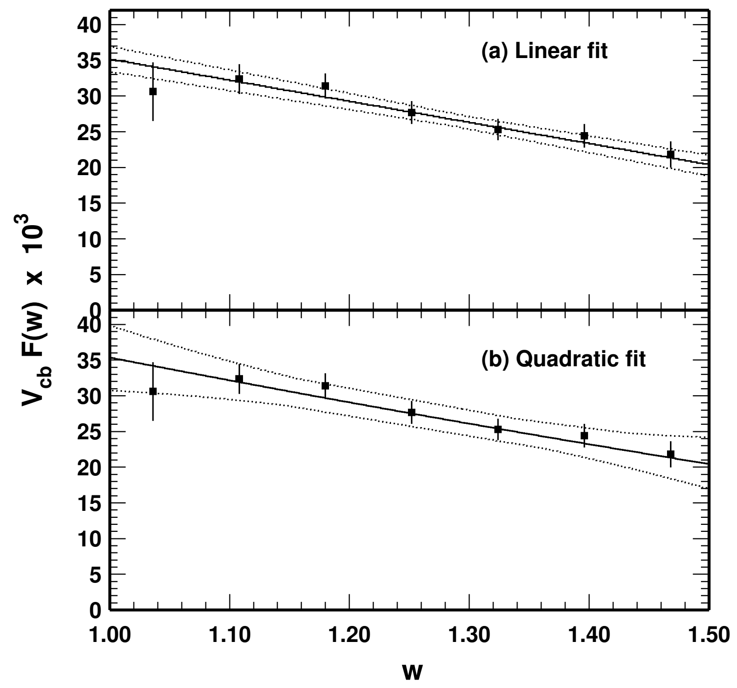

Figure 9: The CLEO data for the decay $B \to D^* \ell \nu$ used to extract $|V_{cb}|$. The data points represent the product $|V_{cb}|F(w)$. Because of smearing in the measurement of w, a small correction is necessary in doing the fits.

ρ^2. Figure 9 shows the fits from CLEO with a linear and quadratic form. Table 3 gives a summary of results for the linear fit. Lattice gauge and model predictions for the parameter $\hat{\rho}^2$ are in the range 0.5-1.0.

To extract $|V_{cb}|$ from these measurements one needs a value of $F(1)$ from theory. If one uses the value $F(1) = 0.93 \pm 0.03$, and the average value of the intercept of the fit, the result is

$$|V_{cb}| = 0.038 \pm 0.002 \pm 0.002. \tag{11}$$

This has somewhat larger statistical error, but smaller systematic error than the result quoted above from the inclusive spectrum. The model error on the inclusive may be overestimated, however. In any case, the agreement is generally quite good, and I will use as an average value

$$|V_{cb}| = 0.039 \pm 0.003. \tag{12}$$

2.2 Measurement of $|V_{ub}/V_{cb}|$

The determination of $|V_{ub}/V_{cb}|$ is perhaps the most important measurement currently being addressed in B physics. The fraction of B semileptonic decays due to the quark decay $b \to c\ \ell\ \overline{\nu}$ is only about 1%, and these modes are therefore very difficult to observe. There is an enormous advantage to looking at lepton energy beyond the $b \to c\ \ell\ \overline{\nu}$ endpoint. Even in this region there is a large background from charm decay leptons. As in the case of $|V_{cb}|$, there are two approaches to measuring $|V_{ub}/V_{cb}|$: inclusive and exclusive.

The first observation of $b \to u$ decays were in the inclusive channel $B \to X_u \ell \nu$ with E_ℓ beyond the endpoint for $B \to X_c \ell \nu$. There is some question about the reliability of models that predict the rate in this small region. Most models predict that it is dominated by a few resonances, but this assumption has been questioned.

The other approach is to study the exclusive modes which are largest in the region beyond the endpoint, which are $B \to \rho(\omega)\ell\nu$. Because the branching ratios are small and the signals hard to find, these are not yet observed. They are worth considering in some detail, however, because the present limits are just at the edge of the level from the inclusive observations. HQET does not predict these decay rates because of the light quark in the final state. There is some relation to D semileptonic decays, however, which may make this method the way to achieve the most precise value of $|V_{ub}/V_{cb}|$ in the long run.

2.2.1 Inclusive $B \to X_u \ell \nu$

The isolation of a $B \to X_u \ell \nu$ signal even in the endpoint region is an extremely challenging analysis. The dominant source of leptons of momentum greater than 2.3 GeV/c at the $\Upsilon(4S)$ is from continuum production of charm. The analysis relies on kinematic cuts which take advantage of the differences between an event with two B mesons decaying at rest and an event with two high momentum charm jets. The value of $|V_{ub}/V_{cb}|$ extracted from the measurement of the excess after these cuts depends strongly on the model used. The models are much less constrained than in the $B \to X_c \ell \nu$ case where heavy quark symmetry must be approximately obeyed.

The fits to the CLEO-II lepton energy spectrum in the endpoint region for both tight and loose cuts are shown in figure 10. There is an excess of events for both plots in the number of leptons from B decays in the momentum region $2.3 - 2.6$ GeV/c. In the range $p_\ell = 2.3 - 2.4$, with tight cuts there are $64 \pm 11 \pm 4$ events from $B \to X_u \ell \nu$; in the range $p_\ell = 2.4 - 2.6$, there are $43 \pm 10 \pm 7$ events. Table 4 shows the measurements of $|V_{ub}/V_{cb}|$ from ARGUS, CLEO-I, and CLEO-II. The ARGUS and CLEO-I results are each based on about $200,000$ $B\overline{B}$ events, and the CLEO-II results are based on about $955,000$ $B\overline{B}$ events. The range of $|V_{ub}/V_{cb}|$ from the CLEO-II analysis is significantly lower than the earlier experiments.

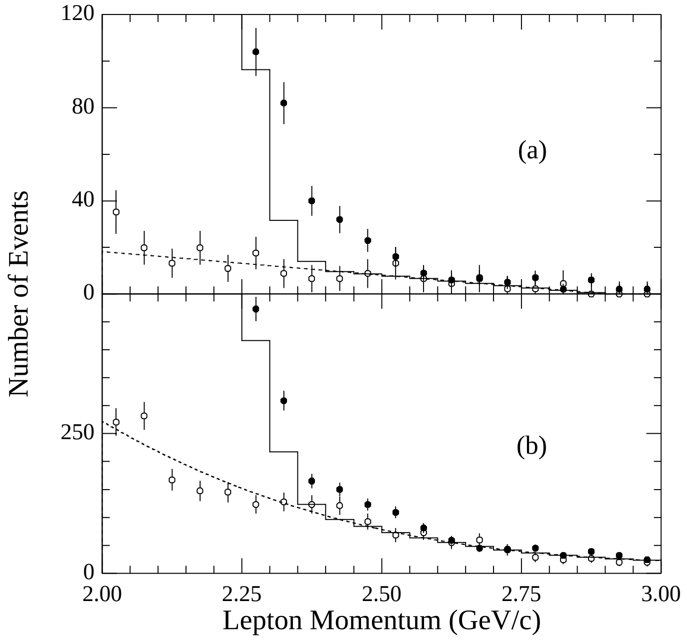

Figure 10: The lepton energy spectrum in the endpoint region from CLEO data, using (a) tight and (b) loose cuts suppressing the continuum background. The filled (open) circles represent the $\Upsilon(4S)$ (scaled continuum) data. The dashed line is the fit to the continuum data, and the solid line is the sum of that fit and the contribution from $B \to X_c \ell \nu$.

2.2.2 Searches for Exclusive Examples of $B \to X_u \ell \nu$

Because the inclusive models may not be reliable in the endpoint region in which we are able to observe $B \to X_u \ell \nu$ decays, it would be very useful to also observe exclusive examples. The exclusive modes which comprise the largest fraction of the semileptonic decays beyond the charm endpoint are $\overline{B}^0 \to \rho^+ \ell^- \overline{\nu}$, $B^- \to \rho^0 \ell^- \overline{\nu}$, and $B^- \to \omega \ell^- \overline{\nu}$. They are expected to occur in the ratio 2:1:1.

CLEO has searched for all three modes but has found no significant signals, leading to the upper limits given in table 5. The known ratios between

Model	ARGUS [18]	CLEO-I [19]	CLEO-II [20]
ACCMM	0.10 ± 0.01	0.09 ± 0.01	0.076 ± 0.008
ISGW	0.18 ± 0.02	0.15 ± 0.02	0.101 ± 0.010

Table 4: Measurements of $|V_{ub}/V_{cb}|$ using the inclusive rate in the endpoint region.

the branching fractions are used to combine the results into a single limit on the branching ratio for either of the two B^- decays. The limit is given for the branching ratio and $|V_{ub}/V_{cb}|$ for three models, giving some indication of the model sensitivity of the result. In the ISGW model, the limit of $|V_{ub}/V_{cb}| < 0.12$ can be compared with the value of 0.101 ± 0.010 from the inclusive measurement. The exclusive limit confirms the lower value of $|V_{ub}/V_{cb}|$ obtained with the CLEO-II inclusive measurement. The sensitivity of the exclusive measurements appear to be just at the threshold of being able to observe significant signals.

model	$B/10^{-4}$	Limit $/10^{-4}$	$\lvert V_{ub}/V_{cb}\rvert^*$
ISGW	$1.0 \pm 0.5 \pm 0.2$	< 1.6	< 0.12
WSB	$1.6 \pm 0.8 \pm 0.3$	< 2.7	< 0.09
KS	$1.3 \pm 0.7 \pm 0.1$	< 2.3	< 0.07

Table 5: Limits on $|V_{ub}/V_{cb}|$ using the exclusive $B^- \to V^0 \ell \overline{\nu}$ decays, where V^0 represents a vector meson, either a ρ^0 or an ω. The results have been corrected to $\tau_B = 1.54$ ps. and $|V_{cb}| = 0.039$.

I will use a value of

$$|V_{ub}/V_{cb}| = 0.076 \pm 0.025. \tag{13}$$

The central value is from the CLEO-II inclusive measurement and the ACCMM model. The error represents the model uncertainty to include the ISGW model. With more data the exclusive modes will start to appear. In addition, with improved understanding of form factors for light quark final states, it may be possible to reduce the model dependence.

2.3 $B^0 - \overline{B}^0$ Mixing

Effectively, two sides of the unitarity triangle are fixed by the measurements of $|V_{ub}|$ and $|V_{cb}|$. For the third side, we need a determination of $|V_{td}|$. For this, we need to make a precise measurement of $B^0 - \overline{B}^0$ mixing.

One can construct the CP eigenstates of the $B^0 - \overline{B}^0$ system in the same way as for K mesons:

$$\begin{aligned} |B_1\rangle &= \left[|B^0\rangle - |\overline{B}^0\rangle\right]/\sqrt{2} \\ |B_2\rangle &= \left[|B^0\rangle + |\overline{B}^0\rangle\right]/\sqrt{2} \end{aligned}$$

If the initial state is pure B_i, and we assume for the moment CP conservation, then the time-dependent wave function is $\psi(t) = |B_i\rangle e^{im_i t} e^{-\Gamma_i t/2}$, (Here m_i

and Γ_i are the mass and width of the B_i.) If one starts with a pure B^0 state, however, the time dependence of the wave function is more interesting:

$$\psi(t) = \left[|B_1\rangle e^{im_1t}e^{-\Gamma_1 t/2} + |B_2\rangle e^{im_2t}e^{-\Gamma_2 t/2}\right]/\sqrt{2}. \tag{14}$$

The relative amplitudes and phases of the two components can change with time, which means that the beam will have some $\overline{B}^0$s. The number of $\overline{B}^0$ at proper time t is given by

$$N_{\overline{B}^0}(t) = N_{B^0}(0)\frac{e^{-\Gamma t}}{2}[\cosh(\Delta\Gamma t/2) - \cos\Delta m t]. \tag{15}$$

Here $\Delta m = m_2 - m_1$, and $\Delta\Gamma = \Gamma_2 = \Gamma_1$. It is convenient to normalize these to the total width, $x_d = \Delta m/\Gamma$ and $y_d = \Delta\Gamma/2\Gamma$.

We can then integrate the time dependence to find the total fraction of neutral B mesons which will decay as a meson of the opposite flavor, χ_d:

$$\chi_d = \left[\frac{\Gamma(B^0 \to \overline{B}^0)}{\Gamma(B^0 \to \overline{B}^0) + \Gamma(B^0 \to \overline{B}^0)}\right] = \frac{x_d^2 + y_d^2}{2 + 2x_d^2}. \tag{16}$$

In the case of B mesons, the mixing is expected to be dominated by the mass difference. This is because, unlike for K mesons, the final states available for the different mass eigenstates to decay into have very similar phase space. So to good approximation, $\chi_d = \frac{x_d^2}{2+2x_d^2}$. In figure 11, the time-dependence of the mixing is shown, for the value $x_d = 0.65$.

It is possible to calculate x_d by starting with the diagrams for $B^0 - \overline{B}^0$ mixing, shown in figure 5. The result is

$$x_d = \frac{G^2\ m_W^2\ m_B\tau_B}{6\ \pi^2}|V_{tb}|^2|V_{td}|^2 f_B^2 B_B M_t^2 F\left[\left(\frac{m_t}{m_W}\right)^2\right]. \tag{17}$$

Here f_B is the decay constant, B_B is a constant often called the bag parameter, and F is a function that decreases slowly with the top quark mass. The dominant uncertainty is in f_B.

B mixing was first discovered by ARGUS looking at dilepton events. This takes advantage of the fact that the lepton charge tags whether the decaying quark was b or $\overline{b}$. Then one measures χ_d using the formula

$$\chi_d = \frac{1}{1-\Lambda}\ \frac{N(\ell^\pm\ell^\pm)}{N(\ell^+\ell^-) + N(\ell^\pm\ell^\pm)}, \tag{18}$$

where $\Lambda = f_+b_+^2/(f_+b_+^2 + f_0b_0^2)$ is the fraction of dilepton events coming from B^+B^- decays. It depends on the semileptonic branching fractions, b_+, b_0, and the production fractions, f_+, f_0. The results of measurements by CLEO [21] and ARGUS[22] using this technique are shown in table 6. The third error listed is due to the uncertainty in Λ.

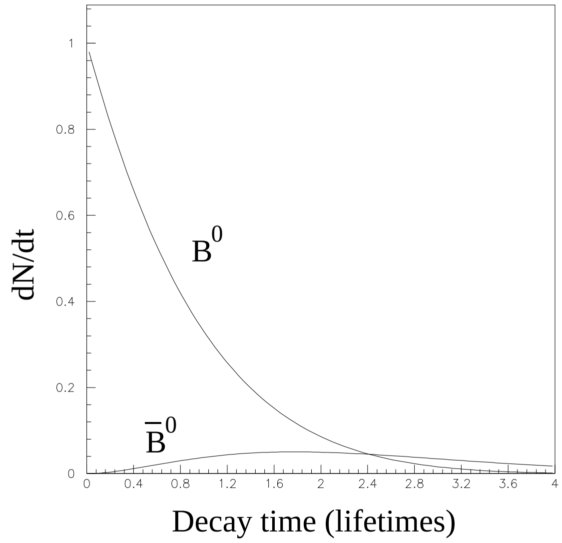

Figure 11: The relative rate of B^0 and $\overline{B}^0$ decays in a beam that is pure B^0 at time zero. The value $x_d = 0.65$ was used for this plot, which corresponds to $\chi_d = 0.149$

Another technique first used by CLEO reduces the uncertainty due to the parameter Λ. It uses the low Q value for the $D^{*+} \to \pi^+ D^0$ decay to tag the D^{*+} without reconstructing the D^0 decay. One uses the approximation $E_{D^*} \approx \frac{E_\pi}{E_\pi^*} M_{D^*}$ and assumes that the D^* momentum points along the π momentum to reconstruct the D^{*+}. One can then do an exclusive search for $\overline{B}^0 \to D^{*+} \ell_1^- \overline{\nu}$, and look for an additional lepton (ℓ_2) in the event. One knows it is a $B^0 \overline{B}^0$ event, and not a $B^+ B^-$ event.

Exp	Tech.	χ_d
CLEO [21]	$2\ \ell$	$0.157 \pm 0.016 \pm 0.018\ ^{+0.028}_{-0.021}$
ARGUS [22]	$2\ \ell$	$0.173 \pm 0.038 \pm 0.044\ ^{+0.031}_{-0.023}$
CLEO [21]	$D^{*+} + \ell$	$0.149 \pm 0.023 \pm 0.019 \pm 0.010$
ARGUS [23]	$D^{*+} + \ell$	$0.16 \pm 0.04 \pm 0.04$
PDG 94	Ave	0.156 ± 0.024

Table 6: The measurements of the B_d mixing parameter χ_d

The additional lepton sample (ℓ_2) is divided into two parts: unlike sign and like sign (relative to the lepton from the $\overline{B}^0 \to D^{*+} \ell_1^- \overline{\nu}$ decay). If there were no mixing, the unlike sign leptons would all be primary leptons from the B decay vertex, and the like sign leptons would all be secondary leptons from the charm daughter of the B. With mixing, there is a small number of like sign primary leptons and unlike sign secondary leptons. The momentum spectra for the additional lepton (ℓ_2) are shown in figure 12. The fits make it possible to extract the fraction of mixed decays. The measurements of χ_d obtained by CLEO [21] and ARGUS [23] using this method are shown in table 6.

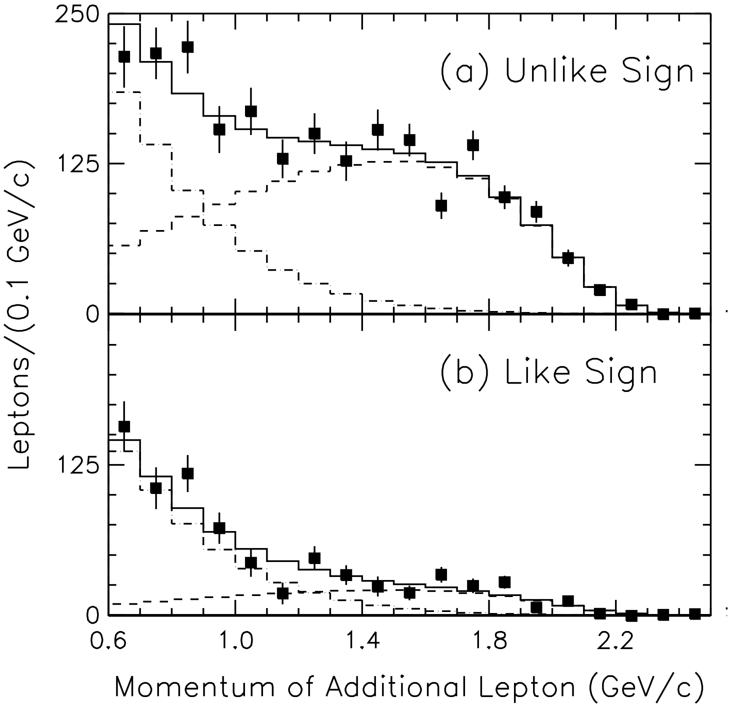

Figure 12: The data from the CLEO mixing measurement using partial reconstruction of the decay $\overline{B}^0 \to D^{*+}\ell_1^-\overline{\nu}$. Shown are the momentum spectra for the additional lepton, divided into samples with charge of sign (a) unlike and (b) like the first lepton. The fit is to the sum of a primary lepton spectrum (dashed line) and a secondary lepton spectrum (dot-dashed line).

The CLEO results are not independent and should not be averaged. We will use the PDG value of $\chi_d = 0.156 \pm 0.024$ for calculating V_{td}. This corresponds to $x_d = 0.67 \pm 0.08$. For the top quark mass, I use $m_t = 165$ GeV. (This is about 8 GeV lower than the pole mass measured by CDF, corresponding to the scaling of the mass with energy scale.) For these values,

$$|V_{td}| = (0.0084 \pm 0.0008) \times \frac{200 \text{ MeV}}{f_B\sqrt{B_B}}. \qquad (19)$$

For $f_B\sqrt{B_B}$, a reasonable value is (190 ± 40) MeV.

At LEP, the B^0 mesons move at high velocity and so it is possible to observe the time evolution of the mixing. Although these measurements are not quite as precise as the best measurements in the table, it is a nice confirmation of our understanding that they agree well with the average from CLEO and ARGUS.

2.4 Experimental Status of the CKM Matrix and the Unitarity Triangle

With the measurements of $|V_{cb}|$, $|V_{ub}|$, and $|V_{td}|$, we have all of the information now available from B mesons on the CKM matrix. As I said at the beginning, there is an additional important constraint on the allowed region of the unitarity triangle from the CP violation parameter ϵ observed in $K_L^0 \to 2\pi$. Using the experimental value of $\epsilon = 2.25 \times 10^{-3}$, one gets a relationship between the CKM parameters η and ρ: [24]

$$\eta = 1.5/\left[\left(\frac{A}{0.8}\right)^2\left(\frac{B_K}{0.8}\right)\left(1+4\left(\frac{A}{0.8}\right)^2(1-\rho)\right)\right] \tag{20}$$

This gives a hyperbola in (ρ, η) space. Since it is the only experimental result used that demands CP violation, it is the only constraint which requires that $\eta \neq 1$.

We now have all of the measurements we need to specify the allowed region for the unitarity triangle. Recall that the triangle is completely specified by the parameters ρ and η, as shown in figure 1.

The experimental information which we need is:

1. $|V_{cb}| = 0.039 \pm 0.003 \Rightarrow A = 0.80 \pm 0.06$.
2. $|V_{ub}/V_{cb}| = 0.076 \pm 0.025$.
3. $|V_{td}| = 0.009 \pm 0.002$.
4. ϵ_K as just discussed.

These measurements lead to the following constraints on ρ and η: (Range is $\pm 1.5\sigma$.):

1. $[\rho^2 + \eta^2]^{1/2} = |V_{ub}/V_{cb}|/\lambda = 0.18 - 0.50$
2. $[(1-\rho)^2 + \eta^2] = |V_{td}|/\lambda|V_{cb}| = 0.75 - 1.45$
3. $1.07/[1 + 3.6(1-\rho)] < \eta < 1.79/[1 + 2.1(1-\rho)]$ (from ϵ_K)

The possible range of unitarity triangles is given by the allowed region in the (ρ,η) plane. Figure 13 shows the allowed region specified by the existing measurements, including errors due to limits of the theory. Note that the area shown is the allowed region only if one assumes that the CP violation seen in K_L decay is due solely to the CKM phase.

The allowed region is smaller than it was three years ago, but it still is rather large. In the last section of these lectures, I will discuss the implications of this figure for the future of CP violation studies in the B^0 system.

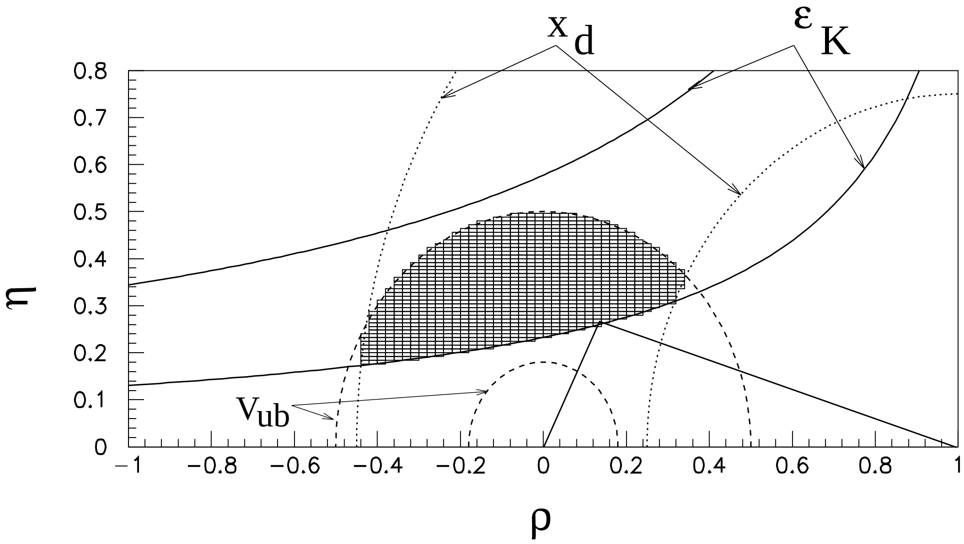

Figure 13: The experimental status of the unitarity triangle. The allowed region for the CKM parameters ρ and η is shaded. An example of an allowed unitarity triangle is shown. The labels show which constraints come from which experimental measurements.

3 MORE INFORMATION FROM B MESON DECAYS

In the previous section I reviewed the measurements using B mesons which determine CKM matrix elements directly. In the last couple years there have been many important results in other decays of B mesons. Some of these, such as lifetimes and form factor measurements, provide supporting information for the CKM measurements, but also offer insights into the structure of heavy mesons. Others give the first look at such hard-to-observe processes as penguin decays. And finally, some of these measurements are needed to plan the round of CP measurements which will take place in the near future.

3.1 Lifetimes

Our first clue that standard model CP violation might be observable in B decays was the discovery of a long B lifetime, corresponding to a small value of $|V_{cb}|$. Precise lifetime measurements are needed for much of B decay physics, such as measuring V_{cb} more accurately. The existing measurements fall in three categories of precision:

1. There are precise measurements of the average B lifetime τ_b, averaged over the mix of $(B^+, B_d^0, B_s^0, \Lambda_b)$ produced at high energies.
2. There are now fairly good measurements of $\tau^+/\tau^0 = \tau(B^+)/\tau(B^0)$ from a number of sources.
3. There are first measurements of $\tau(B_s), \tau(\Lambda_b)$.

I will discuss the first two categories in this section.

3.1.1 Lifetimes of b Hadrons

It is expected that at high energy experiments (LEP, CDF) the mix of hadrons containing the b quark is fairly similar, with perhaps 35% each of B^+ and B_d^0, and 15% each of B_s^0 and Λ_b. The lifetime measurements on such b hadrons are made by the 4 LEP experiments, and by CDF. The two experimental requirements are: a method for selecting a clean sample of b hadrons; and a vertex detector that allows precise measurements of the decay time for each event.

There are three ways to isolate the b sample.

1. At LEP, one selects events with a lepton of high momentum and which has a reasonably high p_T relative to the accompanying jet.

2. In another approach used at LEP, one selects events in which the vertex topology is consistent with 5 separate vertices.

3. At CDF, where a dimuon trigger is required, one uses events with a $\psi \to \mu^+\mu^-$ decays at high transverse momentum.

The most accurate b lifetime measurements are made using silicon vertex detectors. These can provide one-dimensional measurement, such as CDF, or two-dimensional, as at ALEPH.

There are two basic types of decay time measurement. One measures the impact parameter of individual particles, usually leptons; or one finds the vertex for all of the decay products of the B, and then measures the decay distance l. Figure 14 shows the lifetime data from ALEPH, which uses isolated high momentum leptons to select a b-enriched sample, and a three-dimensional impact parameter to measure the decay length [25]. Similar measurements exist from other LEP experiments [26, 27]. Other LEP measurements use vertex topology to select (mostly hadronic) B decays [25, 28]. Figure 15 shows the data from the CDF analysis, which uses events that contain a $\psi \to \mu^+\mu^-$ decay with high transverse momentum. They use the transverse proper decay length to measure the b lifetime [29].

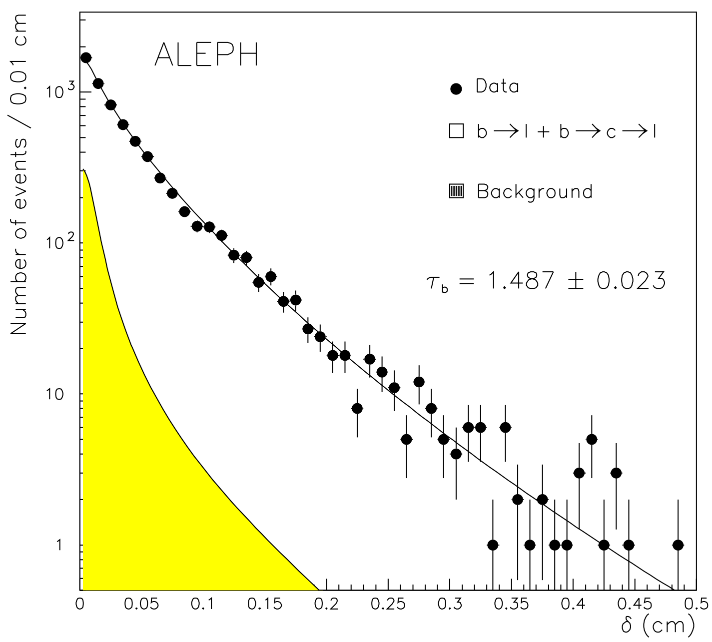

Figure 14: ALEPH Measurement of the average b lifetime.

Table 7 is a summary of the most precise measurements. The average lifetime in the 1994 Review of Particle Properties is $\tau_b = 1.537 \pm 0.021$, which has increased by over four standard deviations from the value of 1.29 ± 0.05

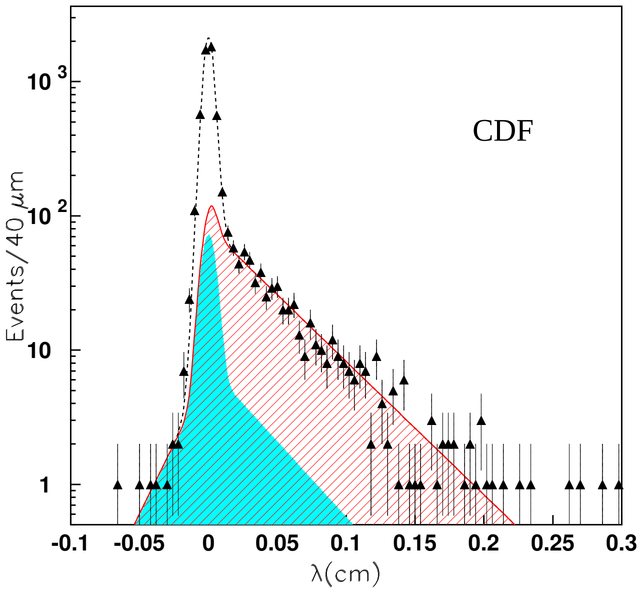

Figure 15: CDF measurement of the average b lifetime.

Exp.	Sample	Technique	τ_b (ps)
CDF	$\psi \to \mu^+\mu^-$	ℓ_T	$1.46 \pm 0.06 \pm 0.06$
ALEPH	both	ip+vert	$1.500 \pm 0.020 \pm 0.050$
L3	leptons	2d ip	$1.535 \pm 0.035 \pm 0.028$
DELPHI	both	ip+vert	$1.582 \pm 0.012 \pm 0.032$
OPAL	leptons	2d ip	$1.523 \pm 0.034 \pm 0.038$
PDG Avg			1.537 ± 0.021

Table 7: Lifetime Measurements for b-flavored Hadrons

ps quoted in the 1992 Review. This means that V_{cb} is reduced by about 9% from that time. In addition, the decay length of the B^0 is increased by about 18%, which makes the measurement of the time evolution of CP violation at a B factory somewhat easier.

At some points in these lectures, where I need to use a B meson lifetime, I use $\tau_B = \tau_b = 1.54$ ps. In fact, there should be a small correction for the part of the b-hadron sample that is B_s or Λ_b. Most recent measurements indicate that the B_s has a lifetime very close to that of the B^+ and B^0. The Λ_b lifetime may be closer to about 1.2 ps, however, which would indicate that $\tau_B \approx 1.03\tau_b$. Since this is a small correction, and the λ_b lifetime is still not well known, I will not use a separate lifetime for the B mesons.

3.1.2 Ratios of B Lifetimes

The ratio $\tau_+/\tau_0 = \tau(B^+)/\tau(B^0)$ is important for a number of reasons. It is needed to measure the semileptonic decay rates, to measure the mixing parameter, and to understand the pattern of hadronic decays. The semileptonic decays of B^+ and B^- are related by isospin: $\Gamma(B^0 \to D^+\ell^-\nu) = \Gamma(B^- \to D^0\ell^-\nu)$. Thus any difference in lifetime is due to a difference in hadronic decay rates.

Why might we expect that the lifetimes are different? It is useful to recall that in the charm sector, there are large differences:

$$\tau(D^+)/\tau(D^0)/\tau(D_s^+) \approx 2.5/1/1$$

We can explain this fact starting with two hypotheses: (a) two-body spectator decays dominate and (b) the ratio of the amplitudes for the two hadronic spectator decays is $a_2/a_1 \approx -0.4$. In that case, $\Rightarrow \frac{\Gamma(D^0 \to \text{had})}{\Gamma(\text{D}^+ \to \text{had})} \approx \frac{|a_1|^2+|a_2|^2}{|a_1+a_2|^2} = 3$, which leads approximately to the observed lifetime ratios. I will discuss this in some detail in the next section.

What are the expectations for B mesons? For one, the scaling to a higher energy scale tends to give a smaller value of $|a_2/a_1|$. Secondly, the 2-body decays do not dominate the inclusive rate. Generally there is a belief that τ_+/τ_0 should be much closer to 1 than is the similar ratio for D's.

Experiments use various methods to tag the sign of the decaying B to measure the lifetime ratio. DELPHI uses a sample of about 800 separated vertices associated with high mass, dividing it into neutral(B^0) and charged(B^+) samples [30]. They then measure the lifetime for each sample, as shown in figure 16. OPAL [31], ALEPH [32], and DELPHI [33] use $D^{(*)}\ell$ combinations to identify the charge of the decaying lepton. $\overline{D}^0\ell^+$ events are predominantly from B^+, $D^-\ell^+$ and $D^{*-}\ell^+$ from B^0. CDF uses exclusive ψX decays [34]. Table 8 shows the direct measurements of τ_+/τ_0, giving an average value of 1.01 ± 0.11.

Exp.	Mode	τ_+/τ_0
DELPHI[30]	topo.	$1.01\ ^{+\,0.29}_{-\,0.22} \pm 0.12$
OPAL[31]	$D^{(*)}\ell$	$1.00\ ^{+\,0.33}_{-\,0.25} \pm 0.08$
ALEPH[32]	$D^{(*)}\ell$	$0.96\ ^{+\,0.19}_{-\,0.15}\ ^{+\,0.18}_{-\,0.12}$
DELPHI[33]	$D^{(*)}\ell$	$1.11\ ^{+\,0.51}_{-\,0.39} \pm 0.11$
CDF[34]	ψ X	$1.02 \pm 0.16 \pm 0.05$

Table 8: Direct Measurements of τ_+/τ_0

The other way to measure the lifetime ratio is to measure accurately the ratio of semileptonic decay branching ratios for B^+ and B^0. Since the decay

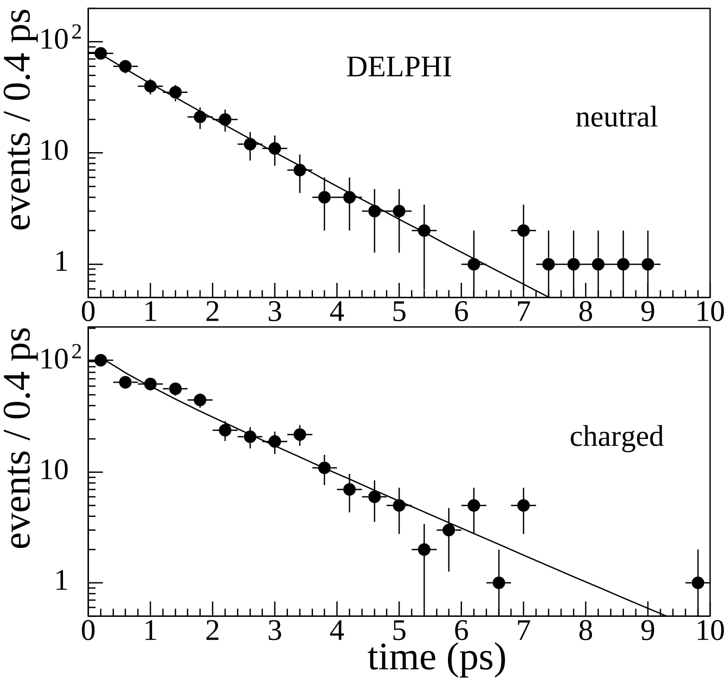

Figure 16: B^+ and B^0 lifetime plots from DELPHI.

rates are equal, $\frac{\tau^+}{\tau^0} = \frac{B(B^+\to\ell^+X)}{B(B^0\to\ell^+X)}$. (A similar technique works with $B \to \psi$ exclusive decays, since the B^+ and B^0 decay rates are related by isospin there as well.) The separation of B^+ from B^0 decays is done at the $\Upsilon(4S)$ by tagging the opposite B, since the event is B^+B^- or $B^0\overline{B^0}$. CLEO tags the other B using hadronic decays such as $B^0 \to D^{*-}\pi^+$, semileptonic decays such as $B^0 \to D^{*-}\ell^+\nu$, and partially reconstructed decays, using the slow pion from the decay $D^{*+} \to \pi^+D^0$ [35]. With this tagging technique, the CLEO measurement does not rely on the assumption of equal production for the charged and neutral Bs. The measurements by CLEO and ARGUS [36, 37] are listed in table 9. The average value of $\tau_+/\tau_0 = 0.95 \pm 0.15$ agrees well with the average of the direct measurements. The Particle Data Group average in the 1994 review is

$$\tau_+/\tau_0 = 0.98 \pm 0.09. \tag{21}$$

Thus the charge and neutral lifetimes are equal to within the present 9% error, which agrees with expectations.

3.2 Form Factors in B Semileptonic Decays

We have already discussed in some detail the measurement of exclusive semileptonic decays. In extracting $|V_{cb}|$ from $\overline{B}^0 \to D^{*+}\ell^-\overline{\nu}$, we are using the concepts of HQET and calculated corrections to the limit of heavy

Exp.	τ_+/τ_0
CLEO[35]	$0.93 \pm 0.18 \pm 0.12$
ARGUS[36]	$1.00 \pm 0.23 \pm 0.14$
ARGUS[37]	$0.91 \pm 0.27 \pm 0.21$

Table 9: Measurements using semileptonic decays

quark symmetry to constrain the form factors. The best opportunity to test our understanding of those corrections is to measure the form factors directly using the full angular distribution.

There are four form factors of interest: the single vector form factor $f_+(q^2)$ in $B \to D\ell\nu$, and the three form factors $A_1(q^2)$, $V(q^2)$, and $A_2(q^2)$ in $B \to D^*\ell\nu$. In HQET, these are all related to a single function $\xi(w)$, where $w = \frac{E_{D^*}}{M_{D^*}} = \frac{M_B^2+M_{D^*}^2-q^2}{2M_BM_{D^*}}$. In particular for the D^* decay, in the heavy quark limit,

$$V = A_2 = \frac{A_1}{1 - q^2/(M_B + M_{D^*})^2} = \xi, \tag{22}$$

and $\xi(1) = 1$. This corresponds to the light degrees of freedom having the same wave function when $b \to c$ at zero recoil.

The statement that $\xi(1) = 1$ in the heavy quark limit does not in itself help the experimenter fit data. One needs to know how large the corrections are at $w = 1$ to the relationships in equation 22, and how $\xi(w)$ evolves away from $w = 1$.

Neubert [38] predicts the ratios of form factors using models to calculate corrections to HQET. His results are

$$\begin{aligned} R_1 &\equiv \left[1 - \frac{q^2}{(M_B + M_{D^*})^2}\right] \frac{V(q^2)}{A_1(q^2)} \approx 1.3 \\ R_2 &\equiv \left[1 - \frac{q^2}{(M_B + M_{D^*})^2}\right] \frac{A_2(q^2)}{A_1(q^2)} \approx 0.8 \end{aligned}$$

A_1 is the dominant form factor in the total rate. It is natural to use ratios of the other form factors to A_1. These ratios can be measured in the experimental data.

We know that the function $\xi(w)$ decreases with increasing w because the wave functions have smaller overlap. A usual parameterization is $\xi(w) = 1 - \rho^2(w-1)$. Lattice gauge calculations find this gives a good fit with $\rho^2 \approx 1$. This is another property of heavy mesons that can be tested experimentally.

CLEO [39] has preliminary results from the first full fit to the angular distribution in $B \to D^*\ell\nu$. The three angles are defined in figure 17. The differential decay rate for $P(Q\overline{q}) \to V(q'\overline{q})\ell^-\overline{\nu}$ can be expressed in terms of

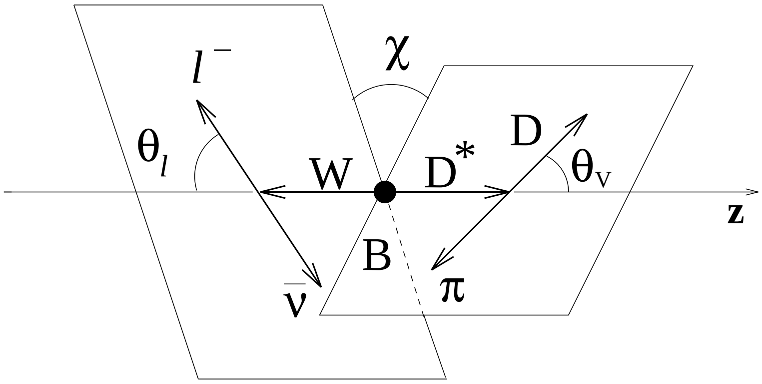

Figure 17: The three angles in the decay $\overline{B}^0 \to D^{*+}\ell^-\overline{\nu}$

these four kinematic variables q^2, θ_ℓ, θ_V and χ [40, 41]:

$$\begin{aligned}
\frac{d\Gamma}{dq^2\, d\cos\theta_V\, d\cos\theta_\ell\, d\chi} &= \frac{3}{8(4\pi)^4} G_F^2 |V_{q'Q}|^2 \frac{p_V q^2}{M^2} \\
&\times \ \{(1-\eta\cos\theta_\ell)^2 \sin^2\theta_V |H_+(q^2)|^2 \\
&+ \ (1+\eta\cos\theta_\ell)^2 \sin^2\theta_V |H_-(q^2)|^2 \\
&+ \ 4\sin^2\theta_\ell \cos^2\theta_V |H_0(q^2)|^2 \\
&- \ 2\sin^2\theta_\ell \sin^2\theta_V \cos 2\chi\, H_+(q^2) H_-(q^2) \\
&- \ 4\eta \sin\theta_\ell (1-\eta\cos\theta_\ell) \sin\theta_V \cos\theta_V \cos\chi\, H_+(q^2) H_0(q^2) \\
&+ \ 4\eta \sin\theta_\ell (1+\eta\cos\theta_\ell) \sin\theta_V \cos\theta_V \cos\chi\, H_-(q^2) H_0(q^2)\}
\end{aligned} \tag{23}$$

where M is the mass of P, p_V is the magnitude of the three-momentum of V in the rest frame of P and is a function of q^2. The factor η is equal to $+1$ for B decays and -1 for D decays.

The helicity amplitudes H_0, H_+ and H_- in equation 23 correspond to the three space-like helicity components of the virtual W. The angular functions in each term are completely determined by the $V-A$ character of the W decay and by the helicities of the virtual W and the vector meson V. The functions of θ_ℓ are the appropriate Wigner d functions, and the functions of θ_V are the appropriate spherical harmonics associated with the orbital angular momentum of the P_1P_2 system. The form factors A_1, A_2 and V are contained in the helicity amplitudes:

$$H_\pm(q^2) \ = \ (M+m_V)A_1(q^2) \mp \frac{2Mp_V}{M+m_V} V(q^2) \tag{24}$$

and

$$H_0(q^2) \ = \ \frac{M+m_V}{2\sqrt{q^2}m_V}[(M^2-m_V^2-q^2)A_1(q^2) - 4\frac{M^2p_V^2}{(M+m_V)^2}A_2(q^2)]. \tag{25}$$

The CLEO data sample consists of about 800 events in the modes $D^* \to \pi^+D^0$, $D^0 \to (K^-\pi^+,\ K^-\pi^+\pi^0)$. In the primary fit, all three quantities,

R_1,R_2, and ρ^2 are allowed to vary. Figure 18 shows the data distributions for the four fit variables. All observed distributions are described well. Table 10 shows the preliminary results for the three variables.

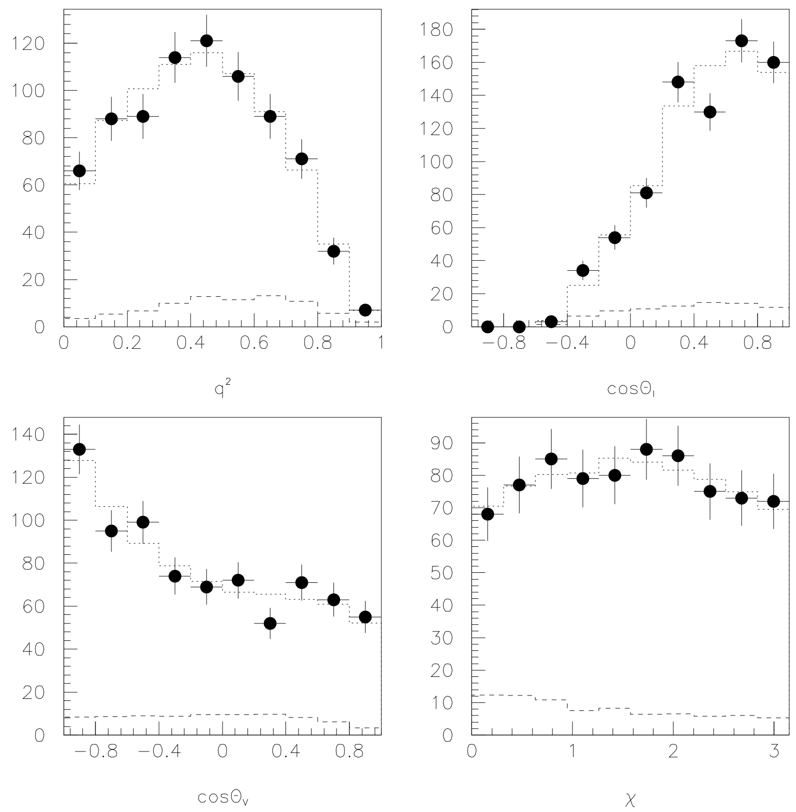

Figure 18: The projections of the four-dimensional fit to the angular distribution in $B \to D^*\ell\nu$ The solid line is the fit, and the dashed line is the contribution from the background.

Fit Parameters	
R_1	$1.30 \pm 0.36 \pm 0.16$
R_2	$0.64 \pm 0.26 \pm 0.12$
ρ^2	$1.01 \pm 0.15 \pm 0.09$

Table 10: The preliminary result of the three parameter fit. The first error is statistical the second is systematic.

This is the first complete measurement of the form factors using all of the information from the decay distribution. The values of R_1 and R_2 obtained agree within errors with the predictions of Neubert [38], $R_1 = 1.3$ and $R_2 =$

0.8. The value of the slope, ρ^2, is within the range expected from lattice QCD or QCD sum rule calculations [42, 43, 44, 38] This encourages one to believe that we are beginning to understand the form factors in $b \to c$ decay at a fairly fundamental level. This is crucial as we try to measure $|V_{cb}|$ ever more precisely, but it is also useful in our attempt to understand the hadronic B decays.

3.3 Hadronic B Decays

There has been a large effort by CLEO in the last couple years to use its large, clean sample of Bs to measure the main exclusive hadronic decays. To illustrate the analysis required, we will consider the reconstruction of the simplest hadronic B Decay: $\overline{B}^0 \to D^{*+}\pi^-$. One looks at events consistent with a spherical $B\overline{B}$-like topology, and reconstructs all possible candidates of $D^0 \to K^-\pi^+, K^-\pi^+\pi^0, K^-\pi^+\pi^-\pi^+$. The next step is to check whether there is a slow π^+ consistent with the $D^{*+} \to \pi^+ D^0$ decay. Then one adds a fast π^- to form a candidate $\overline{B}^0$. One requires $E(D^*\pi) = E_{beam}$ within resolution, which separates modes with an extra pion. Finally, one plots the beam-constrained mass: $M^2 = E_{beam}^2 - p_{D^*\pi}^2$. The beam-constrained mass has a resolution dominated by the beam energy spread, about 2.7 MeV.

One is using the full power of operating at the $\Upsilon(4S)$ in this analysis: There are no extra particles, and the B is at rest. CLEO [45] has recently published results on the major hadronic B decay modes. The signals are quite clean, with about 40 events in each of the best modes. Figure 19 shows the signals for the four decays $B \to D^*\pi^-(\rho^-)$.

The theoretical interpretation of hadronic decays is not as simple as for semileptonic decays, but a simple picture describes them fairly well. In this picture, one assumes the external (a_1) and internal (a_2) spectator decays dominate. The matrix element factorizes into two separate currents, as it does for semileptonic decays. There is a simple relationship between the differential semileptonic rate and the corresponding hadronic rate. In their paper on hadronic decays, CLEO [45] defines the quantity

$$R_{exp} \equiv \frac{\Gamma(B^0 \to D^{*-}\pi^+)}{\frac{d\Gamma}{dq^2}(B^0 \to D^{*-}\ell^+\nu)|_{q^2=m_\pi^2}} \tag{26}$$

If factorization holds, this will be equal to

$$R_{theo} = 6\pi^2|a_1|^2 f_\pi^2 |V_{ud}|^2. \tag{27}$$

This corresponds approximately to taking the amplitude for a semileptonic decay with a q^2 equal to the mass-squared of the light meson in the final state, and multiplying it by the decay constant. It assumes that the final

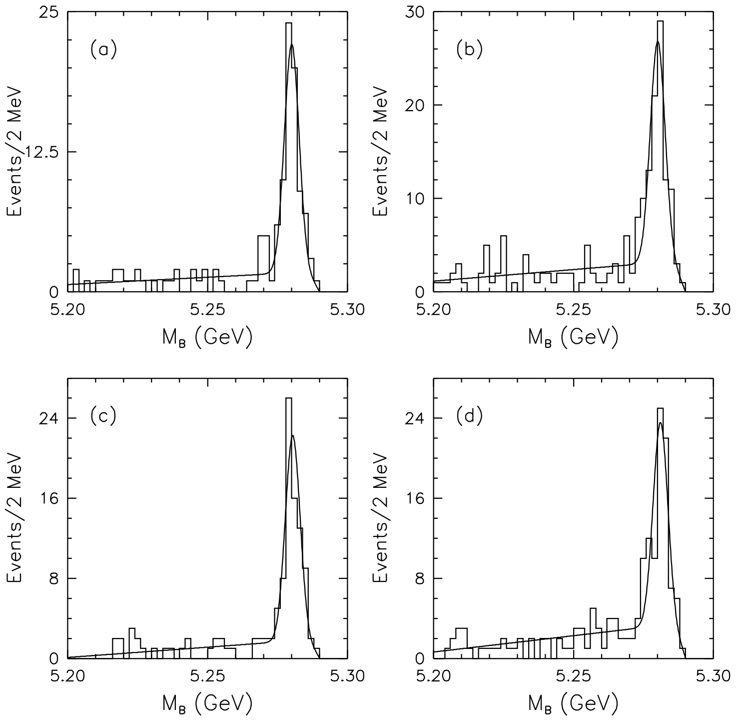

Figure 19: Beam-constrained mass distributions for (a) $B^- \to D^{*0}\pi^-$, (b) $B^- \to D^{*0}\rho^-$, (c) $\overline{B}^0 \to D^{*+}\pi^-$, and (d) $\overline{B}^0 \to D^{*+}\rho^-$ from CLEO.

Mode	$R_{exp}(\mathrm{GeV}^2)$	$R_{theo}(\mathrm{GeV}^2)$
$\overline{B}^0 \to D^{*+}\pi^-$	1.22 ± 0.18	1.22 ± 0.17
$\overline{B}^0 \to D^{*+}\rho^-$	2.96 ± 0.65	3.26 ± 0.46
$\overline{B}^0 \to D^{*+}a_1^-$	3.9 ± 0.9	3.0 ± 0.5

Table 11: Results of the factorization test for three decay modes.

state interactions are negligible, and that the hadronization process for the two mesons in the final state are uncorrelated.

The results are shown in table 11. This simple picture predicts the major B decay modes well, within present 20% experimental errors. This is different from the situation with D decays, as we will see in the next section.

In the unmodified version of the Bauer-Stech-Wirbel scheme, the decay rates can all be expressed in terms of the constant a_1 for external spectator decays and a_2 for internal. This leads to

$$\Gamma(D^+\pi^-)/\Gamma(D^0\pi^0)/\Gamma(D^0\pi^-) \approx |a_1|^2/|a_2|^2/|a_1+a_2|^2$$

In the case of D decays, where $a_2/a_1 \approx -0.4$, this is what causes $\tau(D^+)/\tau(D^0) = 2.5$, as we discussed when talking about lifetime ratios.

It is interesting to measure a_1 and a_2 for two-body B decays. Measuring $|a_1|$ is done using the dominant modes already discussed. The fact that the factorization picture works means that the modes are consistent with a single value of $|a_1|$: $|a_1| = 1.07 \pm 0.04 \pm 0.06$.

Measuring $|a_2|$ is harder. We can try to measure it using decay modes like $\frac{B(\overline{B}^0 \to D^0\pi^0)}{B(\overline{B}^0 \to D^+\pi-)} \approx |a_2/a_1|^2$. The problem is that CLEO is not yet able to see this mode with the present data set [45]. The limit which is closest to the expected branching ratio is $B(\overline{B}^0 \to D^0\pi^0) < 0.035\%$. This is not a very constraining limit, corresponding to $|a_2/a_1| < 0.45$. To determine $|a_2|$, one must instead turn to $B \to \psi K$ decays. These decays are also pure a_2, but are easier to observe because the modes $B^+ \to \psi K^{(*)+}$ and $B^0 \to \psi K^{(*)0}$ have extremely clean signals, as shown in figure 20.

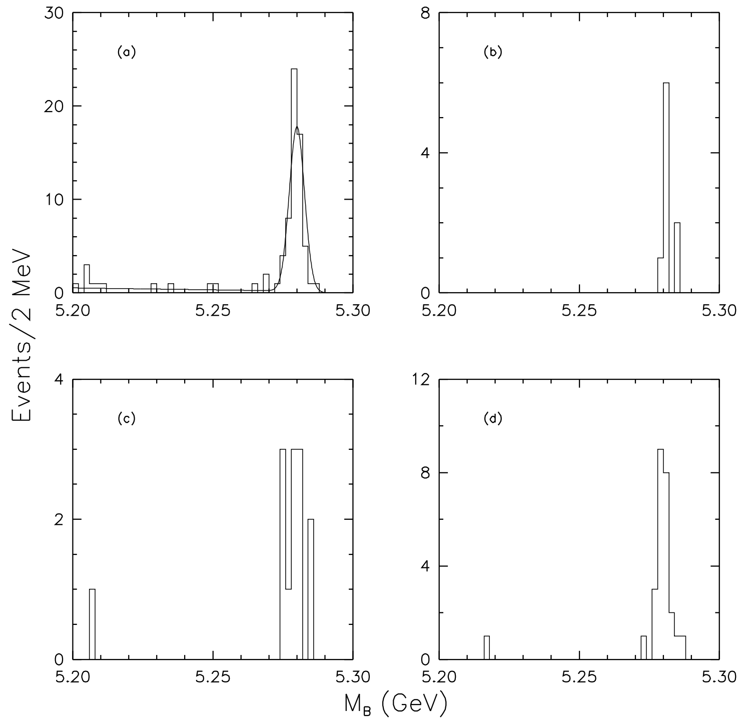

Figure 20: Beam-constrained mass distributions for (a) $B^- \to \psi K^-$, (b) $\overline{B}^0 \to \psi \overline{K}^0$, (c) $B^- \to \psi K^{*-}$, and (d) $\overline{B}^0 \to \psi \overline{K}^{*0}$ from CLEO.

Using these modes, one extracts the result $|a_2| = 0.23 \pm 0.01 \pm 0.01$. Thus, as expected the color-suppressed diagram is smaller than in the case of D decays. Measuring these modes does not determine the sign of a_2, however. Will it be negative, as in the case of Ds?

By comparing the widths for similar B^+ and B^0 modes, one gets a measurement of a_2/a_1, including the sign: $\frac{B(B^+ \to \overline{D}^0\pi^+)}{B(B^0 \to D^-\pi^+)} \approx |1 + a_2/a_1|^2$. CLEO [45]

B^+ Mode	B^0 Mode	$\Gamma(B^+)/\Gamma(B^0)$
$\overline{D}^0\pi^+$	$D^-\pi^+$	1.63 ± 0.36
$\overline{D}^0\rho^+$	$D^-\rho^+$	1.66 ± 0.46
$\overline{D}^{*0}\pi^+$	$D^{*-}\pi^+$	1.86 ± 0.39
$\overline{D}^{*0}\rho^+$	$D^{*-}\rho^+$	2.08 ± 0.61

Table 12: The ratio of decay rates for the major hadronic decay modes from CLEO

has measured the ratio of B^+/B^0 widths for a number of modes. The results are shown in table 12. For B mesons, $\Gamma(B^+)/\Gamma(B^0) \approx 1.9$, corresponding to $a_2/a_1 = 0.27 \pm 0.08 \pm 0.06$. There appears to be clear evidence that $a_2/a_1 > 0$. This disagrees with simple scaling from D decays. It is compatible with some models, however.

It is interesting to note that although for all of the major two-body decay modes, the decay rates for the B^+ are greater than for the B^0, but yet the lifetimes are very nearly the same. Presumably the pattern must reverse for hadronic modes of higher multiplicity.

3.4 Charmless Hadronic Decays

As for the semileptonic decays, a very important goal is the observation of exclusive $b \to u$ hadronic decays, with $B^0 \to \pi^+\pi^-$ a the prime example. With the central value of $|V_{ub}/V_{cb}|$ of 0.08, the branching ratio should be about 1×10^{-5}. Experimentally, this and other $b \to u$ hadronic decays are rare and extremely difficult to observe. The analysis makes use of all of the characteristics of the $\Upsilon(4S)$ environment. The two pions are back-to-back with p = 2.6 GeV/c, and most of the backrounds are from the continuum. There are a number of cuts imposed to reduce this background, cutting on the angle between $\pi - \pi$ axis and thrust axis. on the energy flow of the rest of the event, and on the B momentum direction. Finally, one relies on $\Delta E \equiv E_{\pi^+} + E_{\pi^-} - M_B$ and the beam constrained mass M_B to separate signal from background further.

A second source of charmless B decays is hadronic penguin decay, such as $B^0 \to K^+\pi^-$. The diagram for this mode is shown in figure 4. Again, the expected branching ratio is of order 10^{-5}. In addition, either the $K^+\pi^-$ or the $\pi^+\pi^-$ decay can come from the other diagram, with a rate suppressed by λ^2. Experimentally, K/π separation is only partial at such high momentum, and each mode can be misidentified as the other.

Figure 21 shows the mass spectrum for both $B^0 \to \pi^+\pi^-$ and $B^0 \to K^+\pi^-$ candidates in CLEO [46] data. There is clear evidence of some com-

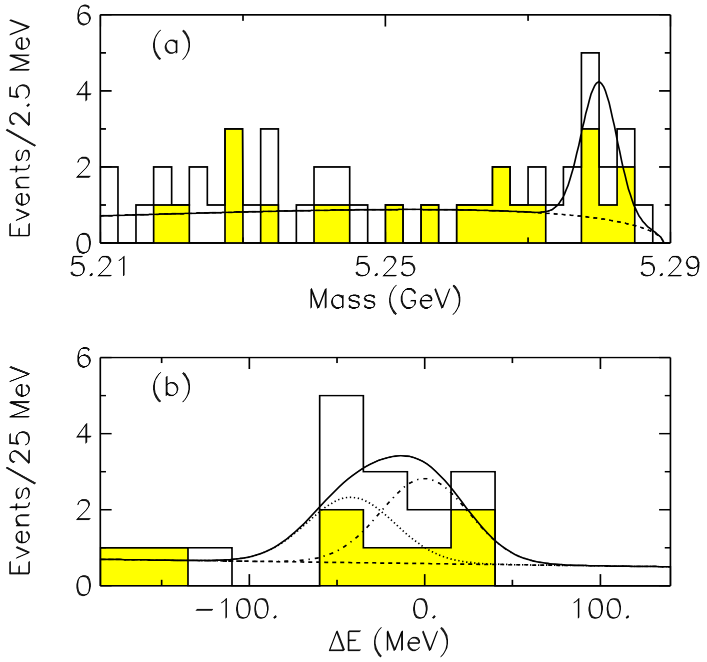

Figure 21: The mass and ΔE plots for the CLEO $B^0 \to \pi^+(K^+)\pi^-$ events. Events identified as $\pi^+\pi^-$ are shaded.

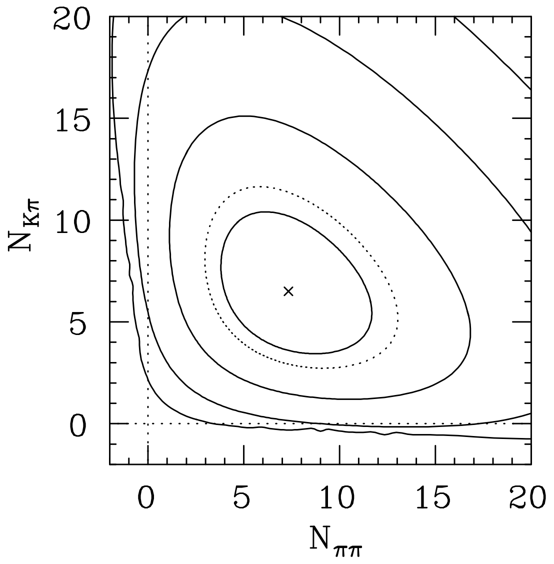

Figure 22: The likelihood contours for the fit to the number of $\pi\pi$ and $K\pi$ decays.

bination of the two decays. The relative fraction of $K^+\pi^-$ and $\pi^+\pi^-$ is not well determined, however. Figure 22 shows the likelihood contours, which demonstrate that the case where both decays are zero is excluded at the five standard deviation level, but that the fraction in either mode can take any value from 0 to 1.

To determine the ratio of these decays is of highest importance in the future program. Let us assume for the moment that the two branching ratios are equal. For the $\pi^+\pi^-$ decay, the penguin amplitude would be about 0.2 times the spectator amplitude, and for the $K^+\pi^-$ decay, the spectator amplitude would be about 0.2 times the penguin. For the study of CP asymmetries in $B^0 \to \pi^+\pi^-$, the interpretation is somewhat more difficult because there is not a single amplitude contributing. We will discuss this "penguin pollution" more in the section on CP violation.

3.5 Electromagnetic Penguin Decays

Figure 4 shows the diagram for the electromagnetic penguin decay. The quark in the loop can be either u, c, or t, but it is dominated by the top quark, and the amplitude is proportional to $V_{tb}V_{ts}$. Higher-order diagrams are important and must be considered in calculating rates. The QCD calculation for $\Gamma(B \to X_s\gamma)$ is fairly well developed, with the result $B_{th}(B \to X_s\gamma) = (3.0 \pm 1.2) \times 10^{-4}$. The allowed range is set by the errors in the top quark mass and in the QCD scale.

The first observation of such an electromagnetic penguin decay was CLEO's observation of the decay $B \to K^*\gamma$ [47]. There is an additional uncertainty in calculating the rate due the form factors for creating a K^*, which are similar those for $B \to \rho\ell\nu$ at zero q^2. The range of theoretical predictions is $B_{th}(B \to K^*\gamma) \approx (2 - 10) \times 10^{-5}$.

At CLEO the signal for this decay is very characteristic: a K^* at the kinematic limit for B decays, E = 2.6 GeV, opposite a γ with about the same energy. Neither of these is possible from the dominant $b \to c$ decay. The major backgrounds are from the continuum, due to $q\overline{q}$ events in which one jet has a leading π^0, or due to initial state radiation of a hard photon. These backgrounds are suppressed with a set of event shape cuts.

Figure 23 shows the CLEO data, in which they observe 13 events in 3 modes, with an expected background of 2.5. This corresponds to $B(B \to K^*\gamma) = (4.5 \pm 1.5 \pm 0.9) \times 10^{-5}$. This established the existence of the electromagnetic penguin decay at about the expected level.

Very recently, CLEO [48] has isolated a signal for inclusive $B \to X_s\gamma$. The signature is a photon with an energy between 2.2 and 2.7 GeV. The background of photons from other B decay processes is small and its size is easy to determine. As in the exclusive decay, the background from continuum

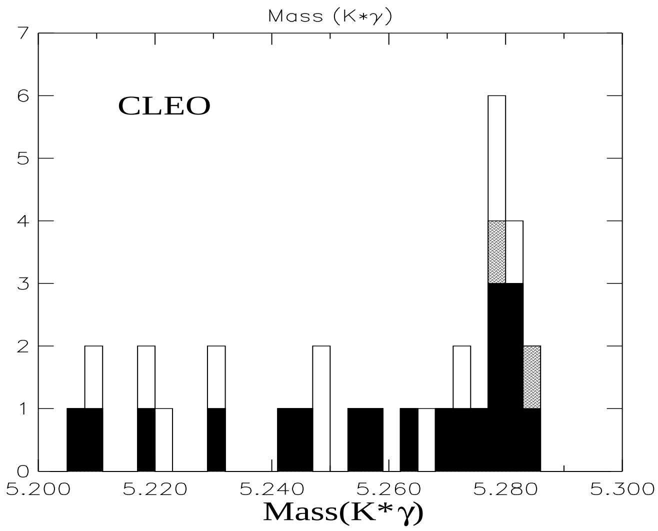

Figure 23: The $B \to K^{*}\gamma$ signal from CLEO.

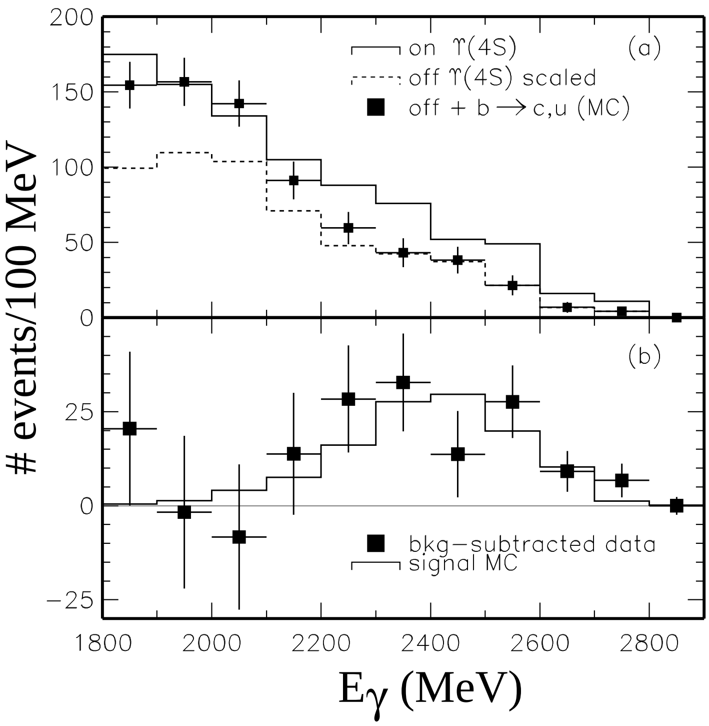

Figure 24: The photon energy spectrum from the CLEO $B \to X_s\gamma$ analysis using B reconstruction.

processes is quite large, and was suppressed with two different techniques.

One technique was to train a neural network which used eight variables which discriminate between $B \to X_s\gamma$ events and continuum events. The second technique was to try to reconstruct at least one exclusive decay, using one of the many known excited K mesons. A significant signal was seen in each approach, with consistent branching ratios. Figure 24 shows the gamma energy spectrum before and after subtraction under the second approach.

The measured branching ratio is

$$B(B \to X_s\gamma) = (2.32 \pm 0.51 \pm 0.29 \pm 0.32) \times 10^{-4}, \tag{28}$$

where the second error is the systematic error from the uncertainty in the yield, and the third error is the multiplicative error from the uncertainty in efficiency, including model dependence. This results is consistent with the calculations based on the penguin diagram. It rules out a charged Higgs lighter than 260 GeV in a two-Higgs doublet model, and it also constrains the parameter space of anomalous $WW\gamma$ couplings in a way that is complementary to the limits from $\overline{p}p \to W\gamma X$ measurements.

3.6 Summary

In this section, I surveyed the status of experimental measurements other than those directly used to determine CKM elements. The main results are

1. The b-hadron lifetime is known very well, and is longer than previously assumed.

2. Detailed fits to extract the form factors in $B \to D^*\ell\nu$ are beginning to test the predictions of HQET with corrections and lattice gauge models of the form factor slope.

3. The dominant two-body hadronic modes are quite well measured. A simple spectator model with $a_1 = 1.07$ and $a_2 = +0.23$ describes the data quite well.

4. Some combination of $B^0 \to \pi^+\pi^- + K^+\pi^-$ is seen, at about the expected level. We need more data to separate the two modes. This separation is very important for future measurements of CP asymmetries.

5. Both exclusive and inclusive electromagnetic penguin decays hae been seen. The level is at the expected level, which rules some region of exotic models.

Some of the information needed to predict the CP measurements is already in hand. Much more will become available in the next three years.

4 CHARM DECAY PHYSICS

4.1 Introduction to Charm Meson Decays

It is 18 years since the discovery of the decays $D^0 \to K^-\pi^+$ and $D^+ \to K^-\pi^+\pi^+$ at SPEAR. The observation of these decays confirmed that the c quark satisfied the predictions of the Glashow-Iliopolous-Maiani (GIM) mechanism; measured the mass of the D mesons; and began the experimental study of weak decays of charm. Since that time a large body of detailed information about charm decays has been collected. The charm decay measurements have come from three types of accelerators: e^+e^- colliders at threshold (SPEAR, BEPC); e^+e^- colliders in the Υ region (CESR, DORIS); and external beams at proton machines (FNAL, SPS).

It is worth reviewing the GIM mechanism and how it predicted the charm quark. The Cabibbo suppression of strange decays was explained by saying that the u quark is the weak partner of the d' quark, defined by the unitary rotation

$$\begin{pmatrix} d' \\ s' \end{pmatrix} = \begin{pmatrix} \cos\theta_c & \sin\theta_c \\ -\sin\theta_c & \cos\theta_c \end{pmatrix} \begin{pmatrix} d \\ s \end{pmatrix}.$$

This scheme could not explain the absence of strangeness-changing neutral currents, as shown in decays such as $K^0 \to \mu^+\mu^-$. The GIM mechanism was proposed to eliminate these currents by postulating a partner for the s' quark, called the charmed quark. The discovery of the charmed quark in 1974, and the observation in 1976 of the decays $D^0 \to K^-\pi^+$ and $D^+ \to K^-\pi^+\pi^+$ dramatically confirmed this picture.

Once the nature of the GIM mechanism was established, much of the effort to understand the weak interactions of quarks naturally turned to the b quark. The question for charm physics became, "What more can one learn from charm decays?" They are not a good place to measure precise CKM parameters ($V_{cs} = V_{ud}$). And one does not expect measurable CP violation in the standard model. The study of charm decays is pointed toward

1. the search for anomalous weak interactions, such as large mixing,
2. the understanding of the nonperturbative strong interactions that are inevitably involved in weak decays of quarks, and
3. the measurement of branching ratios needed for B physics.

The spectator decay diagrams shown in figure 25(a-c) dominate D decays, as they do for B mesons. For the Cabibbo-favored charm decays, the external W diagram corresponds to $D \to \overline{K}(^*)\pi^+(\rho^+)$, and the internal W diagram to $D \to \pi(\rho)\overline{K}^0(\overline{K}^{*0})$. For the case of the D^+, the two diagrams lead to the same final state ($\overline{K}^0\pi^+$, for example.) As discussed in the previous section,

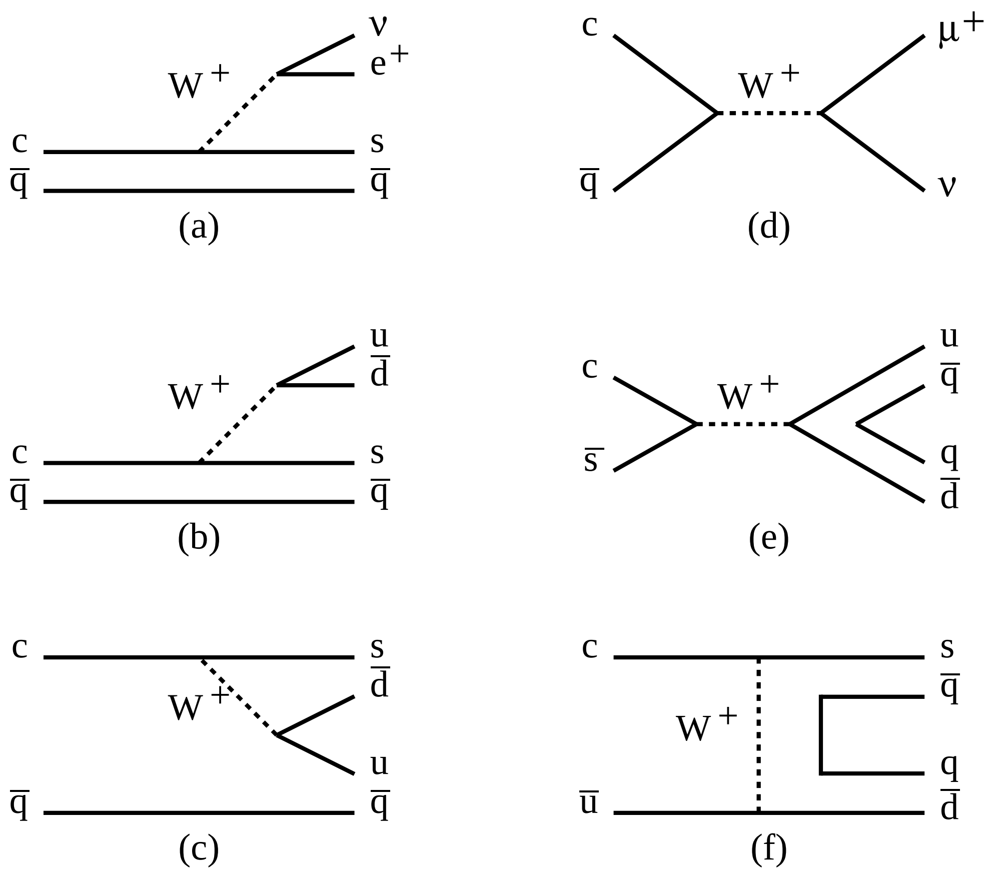

Figure 25: The diagrams for charm meson decays: (a) semileptonic; (b) hadronic spectator, external W; (c) hadronic spectator,internal W; (d) leptonic; (e) W annihilation; and (f) W exchange.

the two diagrams interfere destructively and this increases the D^+ lifetime compared to the D^0 and D_s^+.

The non-spectator diagram in figure 25(d) leads to the helicity-suppressed leptonic decay $D_s^+ \to \mu^+\nu$, which we will discuss later. Hadronic non-spectator decays, figures 25(e-f) lead to the decays $D_s^+ \to \rho^0\pi^+$ and $D^0 \to \phi K^0$. The strong interactions can mitigate the helicity suppression somewhat, but these decays still have a rather small effect on the inclusive hadronic rate. This is not true for the charm baryons, however, where there is no helicity suppression. W-exchange diagrams lead to the very short lifetime for the Λ_c^+.

4.2 Charm lifetimes

The simple picture of two-body spectator decays with destructive interference explains the main features of the D lifetimes rather well. The ratio of the amplitudes for the two diagrams is measured to be $a_2/a_1 \approx -0.4$. This leads to an expected ratio of hadronic widths $\Gamma_{had}(D^0)/\Gamma_{had}(D^+) \approx 3$, and to a ratio of lifetimes $\tau(D^+)/\tau(D^0) \approx 2.5$.

The charm lifetime measurements are dominated by the fixed target experiments, especially Fermilab E-687 and the now old E-691. The general procedure used to isolate a charm signal in such experiments is to select, for example, two tracks which the Cerenkov counters identify as consistent with $D^0 \to K^-\pi^+$. Then some basic cuts are applied to reduce background, requiring: 1) high momentum, 2) a good vertex for the K, π tracks, 3) the K, π vertex to be separated from the primary vertex, and 4) the D^0 momentum direction to point from the primary to the secondary vertex. For decays with higher backgrounds, more stringent cuts can be used, but these are adequate for the major modes used for lifetime measurements, such as $D^0 \to K^-\pi^+$, $K^-\pi^+\pi^0$, and $K^-\pi^+\pi^-\pi^+$; $D^+ \to K^-\pi^+\pi^+$; and $D_s^+ \to \phi\pi^+$ and $\overline{K}^{*0}K^+$. In addition, one can get a cleaner sample of the D^0 decays by requiring a slow pion consistent with the decay $D^{*+} \to \pi^+ D^0$.

Figure 26 shows the mass peak for the $D^+ \to K^-\pi^+\pi^+$ signal from E-687. There are 9196 D^+ decays with a signal to background ratio of about 15 at the peak. This number is about 0.03 before the vertex cuts, so the relative suppression of the background is a factor of about 500. Table 13 shows a summary of the lifetime measurements for the three D mesons.

Exp.	D^+	D^0	D_s^+
E-687 [49]	$1.048 \pm 0.015 \pm 0.011$	$0.413 \pm 0.004 \pm 0.003$	$0.475 \pm 0.020 \pm 0.007$
E-691 [50]	$1.090 \pm 0.030 \pm 0.025$	$0.422 \pm 0.008 \pm 0.010$	$0.47 \pm 0.04 \pm 0.02$
PDG Ave	1.057 ± 0.015	0.415 ± 0.004	0.467 ± 0.017

Table 13: Lifetime measurements for D mesons (psec)

The errors from the E-687 lifetime measurements are about a factor of two better than that of the E-691 data taken in 1985. Together, they dominate the world average. The precision of the lifetime measurements is beyond the ability to calculate them, but precise lifetime ratios are important, especially when comparing decay rates of the different charm mesons. Using the average lifetimes, the ratios are $\frac{\tau(D^+)}{\tau(D^0)} = 2.55 \pm 0.05$ and $\frac{\tau(D_s^+)}{\tau(D^0)} = 1.13 \pm 0.05$.

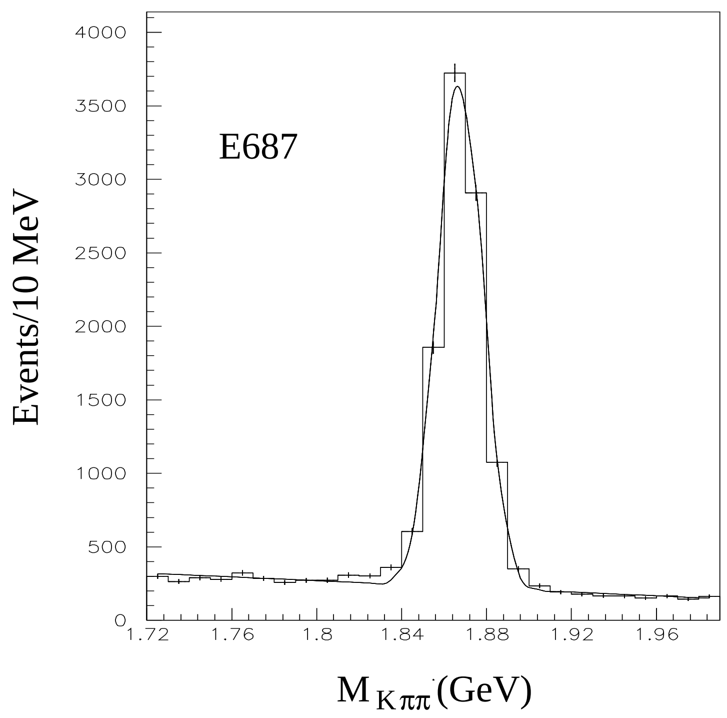

Figure 26: D^+ signal from E-687

4.3 Hadronic Branching Fractions

Since the initial discovery of D meson decays, the benchmark modes for normalizing the branching fractions have been $D^0 \to K^-\pi^+$ and $D^+ \to K^-\pi^+\pi^+$. For many problems in B physics, such as the branching ratios for the major hadronic and semileptonic decays, there has been a significant systematic error associated with these absolute branching fractions.

CLEO-II has recently completed measurements of both absolute branching fractions using a the slow pion from $D^* \to \pi D$ decay to tag the number of D decays inclusively. They use charm produced directly in $c\bar{c}$ events, which have a clear dijet structure. The D^* has a typical momentum of about 3 GeV/c, which is close to the thrust axis. The slow pion has a momentum of about 40 MeV/c in the D^* frame. As a result, the transverse momentum $p \sin\alpha$, where α is the angle of the pion relative to the thrust axis, is about 50 MeV/c. Figure 27 shows the distribution of $\sin^2\alpha$ for eight momentum bins. There are clear peaks at zero angle associated with the decay $D^{*+} \to \pi^+ D^0$. When one looks for the decay $D^0 \to K^-\pi^+$ associated with that decay, one gets the peak shown in figure 28. Table 14 shows the best measurements of the absolute branching fractions for both D^0 and D^+, and the recently published world average.

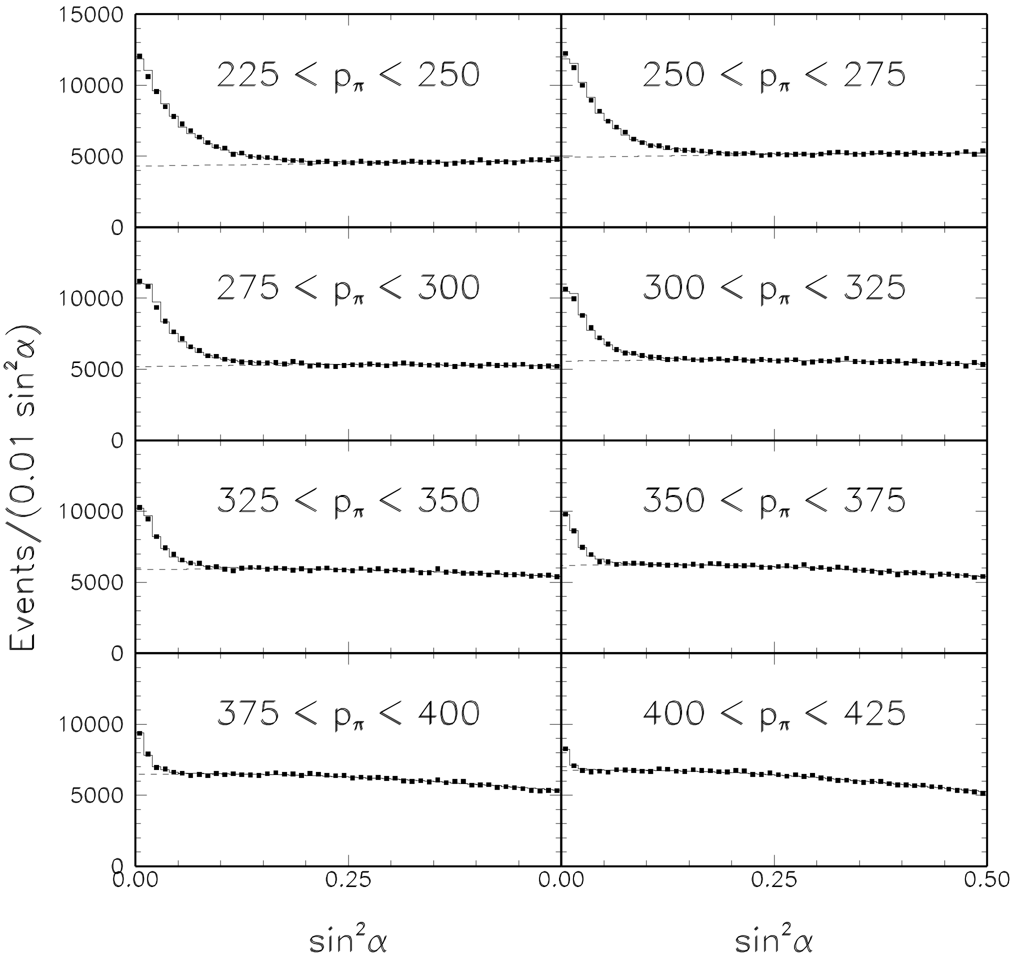

Figure 27: Plots of $\sin^2\alpha$ for low momentum pions from CLEO data. The momentum region for each plot is shown.

A great number of individual hadronic charm decays have been measured by now, so that it is possible to account for all of the major contributors to the total rate. The simple picture of spectator decays plus interference explains the lifetime pattern for D mesons and the general pattern of branching ratios. There are, however, discrepancies between such a picture an the measurements for individual modes at the factor of 2 level. Such a picture does not take into account final state interactions, which we know to be large in the few modes for which we can measure them. This is very different from the case in B decays, where final state interactions can be neglected, to the present experimental accuracy.

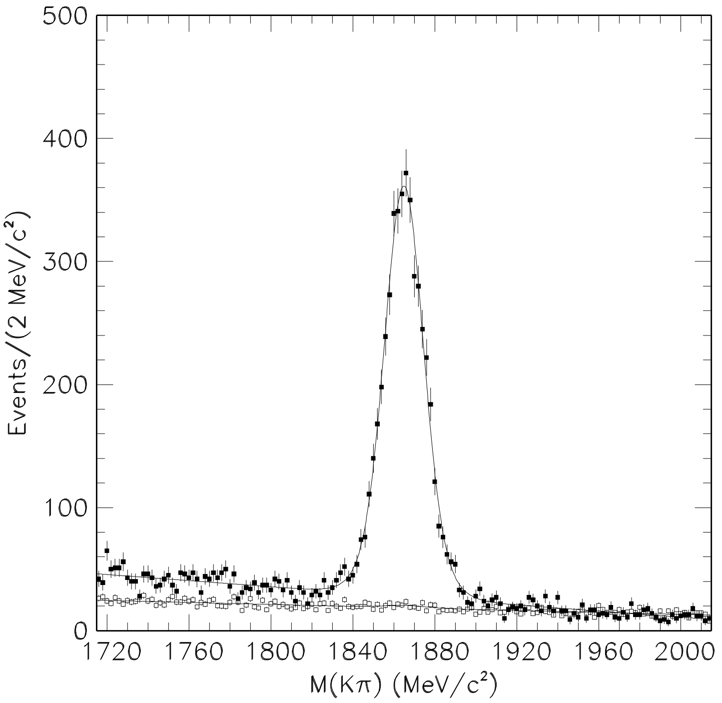

Figure 28: $D^{*+} \to \pi^+ D^0, D^0 \to K^- \pi^+$ signal from CLEO

Exp.	$B(D^0 \to K^-\pi^+)$ (%)	$B(D^+ \to K^-\pi^+\pi^+)$ (%)
CLEO II [51]	$3.91 \pm 0.08 \pm 0.17$	$9.3 \pm 0.6 \pm 0.8$
ARGUS [52]	$4.33 \pm 0.15 \pm 0.40$	
Mark III [53]	$4.2 \pm 0.4 \pm 0.4$	$9.1 \pm 1.3 \pm 0.4$
PDG Ave [9]	4.01 ± 0.14	9.1 ± 0.6

Table 14: Measurements of Absolute Charm Branching Fractions

4.4 $D^0 - \overline{D}^0$ Mixing

Exclusive charm decays with $\Delta C = -\Delta S$, such as $D^0 \to K^+\pi^-$, are both rare and interesting. There are two separate mechanisms that can lead to such decays: (a) mixing, in which $D^0 \to \overline{D}^0 \to K^+\pi^-$; and (b) doubly Cabibbo suppressed decays (DCSD), in which $D^0 \to K^+\pi^-$ directly.

As for the case of B^0 mixing, we define $x = \Delta M/\Gamma$ and $y = \Delta\Gamma/\Gamma$. In the Standard Model, D^0 mixing is expected to be very small. The dominant D^0 decays are Cabibbo-favored, and the heavy quark in the usual mixing loop diagram (see figure 29) is a b quark, rather than a t quark. From this quark box diagram, one expects $r_m = (x^2 + y^2)/2$, the ratio of mixed to unmixed decays, to be in the range 10^{-7}. Theorists have suggested there might be mixing as high as at the $r_m \approx 10^{-4}$ level. This would occur because

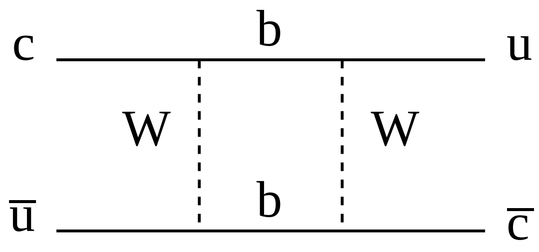

Figure 29: A diagram for $D^0 - \overline{D}^0$ mixing.

the different real decay final states for the two CP eigenstates would lead to $\Delta\Gamma \approx 10^{-2}\Gamma$. Recently, this argument has been called into question by other theorists who argue that r should in fact be very small. If this were true, observation of mixing at the higher level would be an indication of new physics.

The corresponding parameter for DCSD is r_{DC}, which is the ratio of wrong sign to right sign decays at zero decay time, or assuming no mixing. One expects $r_{DC} = \tan^4\theta_c = 0.0026$, but variations of a factor of 2 or more are possible.

Most experiments use the process $D^{*+} \to \pi^+ D^0$ to tag the flavor of the D at production. (Mark III uses doubly tagged events, since the ψ'' is below D^* production threshold.) One way to separate mixing and DCSD is the different time dependence. The DCSD events follow the usual $e^{-t/\tau}$ evolution, while the rate for mixed events is zero at small times and grows like $t^2e^{-t/\tau}$ in the limit of small mixing.

The fixed target experiments cut out events with small lifetime to reduce backgrounds anyway, so they are well-matched to the study of mixing. E-691 keeps events with a decay time greater than $2\tau(D^0)$, which keeps 68% of the mixed events and only 14% of DCSD events. They get the best published limit of $r_m < 0.0037$ ([54]), although E-687 and E-791 should reach sensitivity better by about a factor of two when they finish the mixing analysis on their full data sets.

CLEO does not use information on the decay time, and is sensitive to the sum of mixing and DCSD. They observe the process $D^{*+} \to \pi^+ D^0, D^0 \to K^+\pi^-$ [55]. Events consistent with the Cabibbo-allowed or singly suppressed decays are explicitly vetoed. The remaining signal, which is shown in figure 30 is 19 ± 6 events, compared to 2465 $D^0 \to K^-\pi^+$ events. The result is $r_{DC} = (0.77 \pm 0.25 \pm 0.25)\% \approx 3\ \tan^4(\theta_C)$. Since this is significantly larger than the mixing limit, it must be predominantly due to DCSD. Unfortunately, this rather high DCSD rate will make it harder to improve the sensitivity for mixing.

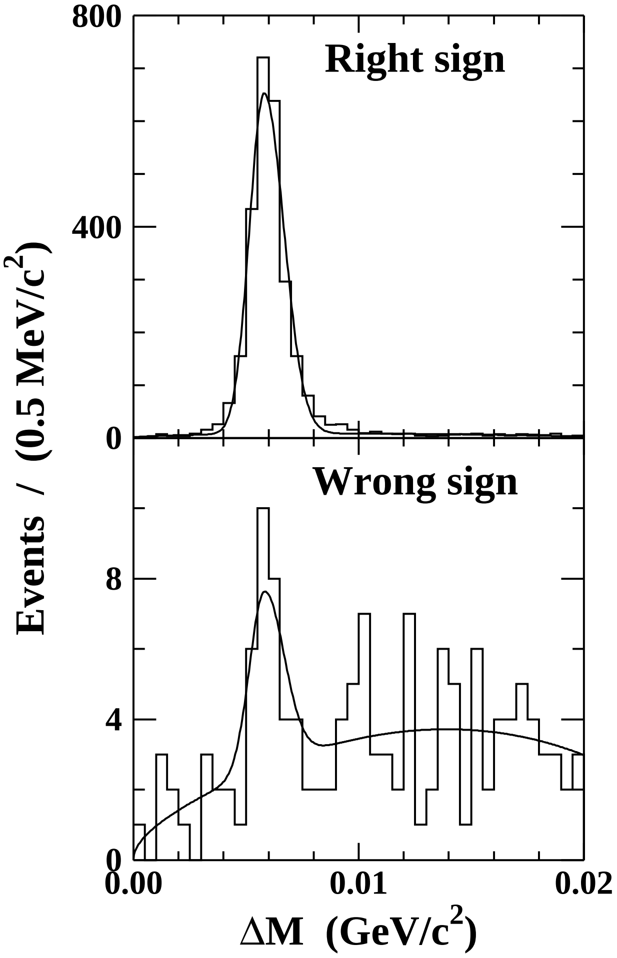

Figure 30: Signals for $D^{*+} \to \pi^+ D^0$, (a) $D^0 \to K^- \pi^+$ and (b) $D^0 \to K^+ \pi^-$ from CLEO.

4.5 Semileptonic Decays

As discussed in section 2, semileptonic decays are especially interesting because they are the easiest to interpret. The diagram is shown in figure 25. The form factors are as described for B decay: for the $D \to K$ transition there is a single vector form factor $f_+(q^2)$; and for $D \to K^*$ there are three form factors, $A_1(q^2)$, $V(q^2)$, and $A_2(q^2)$. The rates for the Cabibbo-allowed decays of the D^0 and D^+ are related by isospin, $\Gamma(D^0 \to K^- \ell^+ \nu) = \Gamma(D^+ \to \overline{K}^0 \ell^+ \nu)$ and $\Gamma(D^0 \to K^{*-} \ell^+ \nu) = \Gamma(D^+ \to \overline{K}^{*0} \ell^+ \nu)$.

The CKM matrix element for $c \to s \ell \nu$ is known, and we want to measure the form factors, and check against theoretical calculations. We would like

Exp.	Lepton	Norm. Mode	$B(D^0 \to K^- e^+ \nu)\%$	m_p GeV/c^2
E691 [57]	e	$D^0 \to K^-\pi^+$	3.64 ± 0.54	$2.1^{+0.4}_{-0.2} \pm 0.2$
CLEO-I [58]	e	$D^0 \to K^-\pi^+$	3.60 ± 0.37	$2.1^{+0.4+0.3}_{-0.2-0.2}$
CLEO-I* [58]	μ	$D^0 \to K^-\pi^+$	3.26 ± 0.50	
E687* [59]	μ	$D^0 \to K^-\pi^+$	3.38 ± 0.75	
CLEO-II* [56]	e, μ	$D^0 \to K^-\pi^+$	3.91 ± 0.25	$2.00 \pm 0.12 \pm 0.18$
PDG Ave [9]			3.69 ± 0.21	

*Muon measurements have been scaled up by 1.03 to be equivalent to electrons.

Table 15: Measurements of the $D^0 \to K^- e^+ \nu$ branching fraction.

to measure the form factors for $D \to K(K^*)\ell\nu$ very well, and relate them to those for $B \to \pi(\rho)\ell\nu$ at high q^2. This might be done through HQET [1], lattice gauge calculations, or quark sum rules.

The largest and best measured semileptonic decay is $D \to K\ell\nu$. Table 15 shows the summary of a series of experiments which measure $R_0 = \frac{B(D^0 \to K^- \ell^+ \nu)}{B(D^0 \to K^- \pi^+)}$ and use this to determine $B(D^0 \to K^- \ell^+ \nu)$. The largest sample is the recent measurement by CLEO [56]. Figure 31 shows the results of the CLEO analysis, which made use of the decay process $D^{*+} \to \pi^+ D^0, D^0 \to K^- \ell^+ \nu$. The mass difference $\delta m = m(K\ell\pi) - m(K\ell)$ shows the characteristic peak near the pion mass that is seen for hadronic decays, although it is somewhat broadened because of the missing neutrino. The $D^0 \to K^- \ell^+ \nu$ sample includes 2510 events, corresponding to a measurement of $B(D^0 \to K^- \ell^+ \nu)$ with 3% statistical and 5% systematic error.

The goal of measuring the decay $D^0 \to K^- \ell^+ \nu$ is to determine the form factor $f_+(q^2)$, which represents the amplitude that the $(s\overline{q})$ state forms a K meson. At $q^2 = q^2_{max} = (M_D - M_K)^2$, the K is at rest in the D frame. The differential decay rate for $D \to K\ell\nu$ has the same form as for $B \to D\ell\nu$:

$$\frac{d\Gamma}{dq^2} = \frac{G^2}{24\pi^3} \, |V_{cs}|^2 \, P_K^3 \, f_+^2(q^2). \tag{29}$$

From the branching fraction and the lifetimes already quoted, one can calculate the decay rate, $\Gamma(D^0 \to K^- e^+ \nu) = (8.9 \pm 0.5) \times 10^{10}\mathrm{s}^{-1}$. This determines the normalization of the form factor: $f_+(0) = 0.77 \pm 0.04$. I will compare this with theoretical predictions below.

The shape of the form factor is a measure of the decreasing overlap of the D and K wave functions as E_K increases. CLEO has measured this shape with the large $D^0 \to K^- \ell^+ \nu$ sample. The dominant q^2 dependence in the rate is from the P_K^3 term in equation 29, which causes the differential decay rate to peak at low q^2. The factor $f_+^2(q^2)$ increases with q^2, changing by a factor of about 2 over the kinematic range of the decay.

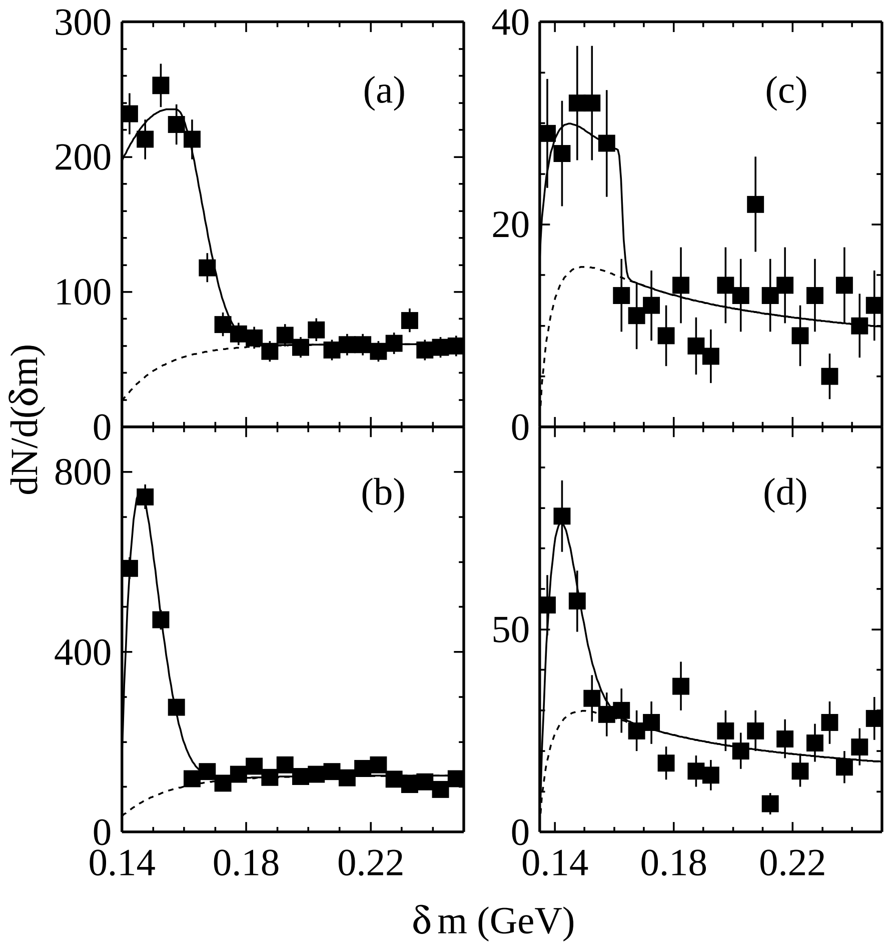

Figure 31: Signals for $D \to \overline{K}\ell^+\nu$ from CLEO. The process observed is $D^* \to \pi + D, D \to K\ell\nu$, and $\delta m = m_{K\ell\pi} - m_{K\ell}$. The plots are for D^0 , $m_{K\ell}$= 1.2-1.4 GeV (a) and 1.4-1.8 GeV (b); and $D^+, m_{K\ell}$= 1.2-1.4 GeV (c) and 1.4-1.8 GeV (d).

Figure 32 shows the measured q^2 spectrum for the $D \to \overline{K}\ell^+\nu$ candidates. A good fit to the data is obtained with the form $f_+(q^2) = f_+(0)/(1-q^2/M^{*2})$, with $M^* = (2.00 \pm 0.12 \pm 0.18)$ GeV, which is in good agreement with the value of 2.1 GeV expected from the closest resonance with the proper quantum numbers, the D_s^*. Other measurements of this pole mass are included in table 15

There have been a number of measurements of $B(D \to K^*\ell^+\nu)$, with both D^0 and D^+ mesons. Table 16 shows measurements of the decay rate $\Gamma(D \to K^*\ell^+\nu)$. I have used for each experiment the branching ratio relative to the normalization mode listed, and the average from this review for the normalization mode. The average value from these measurements is $\Gamma(D \to K^*\ell^+\nu) = (5.1 \pm 0.5) \times 10^{10}\mathrm{s}^{-1}$, which is substantially lower than the early predictions.

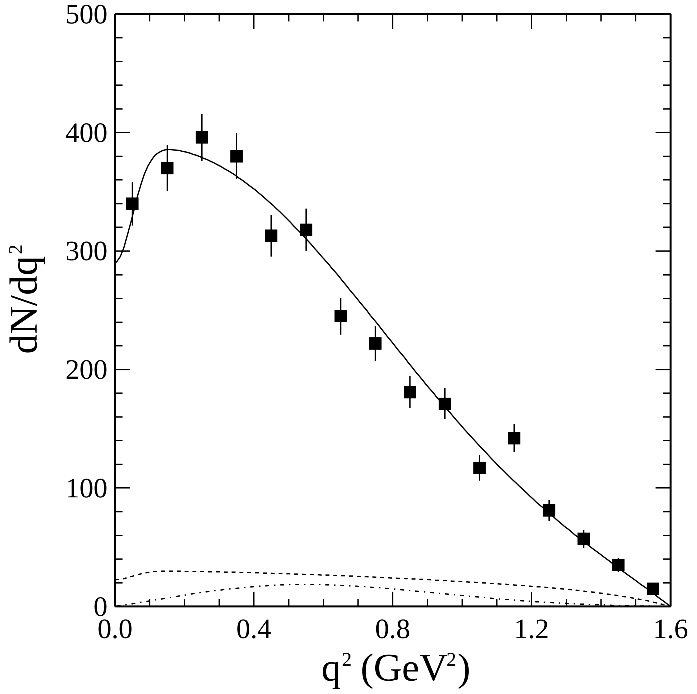

Figure 32: The fit to the q^2 distribution for the CLEO $D^0 \to K^-\ell^+\nu$ sample

To understand the low value of $\Gamma(D \to K^*\ell^+\nu)/\Gamma(D \to \overline{K}\ell^+\nu)$, one must look at the form factors directly. The amplitude for semileptonic decay to a vector meson has three form factors, as for $B \to D^*\ell\nu$. The rate is dominated by the A_1 form factor. The ratios of form factors are determined by fitting the angular distributions, in a way analogous to that described for B decay. In the fits made to date, it has been assumed that the q^2 dependence of the form factors follows that of the $K\ell\nu$ form factor. The form factor results are shown in table 17. As the precision of the measurements improve, the correctness of this assumption will have to tested.

With all of these measurements, we have accurate measurements of two form factors, f_+ and A_1, and coarser measurements of V and A_2. The goal is to compare a complete set of these form factor measurements with the various calculations, either using quark models, lattice gauge calculations, or quark sum rules. This is done in table 18. The ratios of form factors, which may be more reliably predicted, can also be compared using this table.

Certain conclusions can be reached from table 18. For f_+, most calculations agree with data, although the LMMS and BBD versions are somewhat low. The calculations of A_1 are mostly high by a factor of 1.4 or so, which corresponds to about a factor of two in rate. The exceptions are LMMS and BBD, which agree rather well. For V, almost all of the calculations agree within the present large errors. Finally, the quark model estimates of A_2 are generally high, although the other methods agree within large experimental

Exp	$K^*\ell\nu$ mode	normalization	$\Gamma(D \to K^*\ell^+\nu)$ ($10^{10}\mathrm{s}^{-1}$)
CLEO-II [56]	Both	$K^-\pi^+$	5.7 ± 0.7
E-687 [60]	D^+	$K^-\pi^+\pi^+$	5.0 ± 0.9
E-691 [61]	D^+	$K^-\pi^+\pi^+$	4.4 ± 0.8
E-653 [62]	D^+	$K^-\pi^+\pi^+$	4.2 ± 1.2
ARGUS [63]	D^+	$K^-\pi^+\pi^+$	5.0 ± 1.3
CLEO 1.5 [58]	D^0	$K^-\ell^+\nu$	4.6 ± 1.7
Ave			5.1 ± 0.5

Table 16: Measurements of $\Gamma(D \to K^*\ell^+\nu)$. The normalization values used were $\Gamma(D^0 \to K^-\pi^+) = (9.3 \pm 0.4) \times 10^{10}\mathrm{s}^{-1}$ (CLEO II); $\Gamma(D^0 \to K^-\ell^+\nu) = (9.0 \pm 0.5) \times 10^{10}\mathrm{s}^{-1}$ (CLEO 1.5); and $\Gamma(D^+ \to K^-\pi^+\pi^+) = (9.0 \pm 1.0) \times 10^{10}\mathrm{s}^{-1}$ (others).

Exp.	$R_v = V/A_1$	$R_2 = A_2/A_1$
E-687 [60]	$1.74 \pm 0.27 \pm 0.28$	$0.78 \pm 0.18 \pm 0.10$
E-653 [64]	$2.00 \pm 0.33 \pm 0.16$	$0.82 \pm 0.22 \pm 0.11$
E-691 [61]	$2.0 \pm 0.6 \pm 0.3$	$0.0 \pm 0.5 \pm 0.2$
Ave	1.90 ± 0.25	0.74 ± 0.15

Table 17: Form Factor Ratios in $D \to K^*\ell^+\nu$

and theoretical errors.

With all of this experimental information on semileptonic D decays, we can inquire whether the pseudoscalar and vector mesons dominate the inclusive semileptonic rates. Table 19 summarizes the experimental information. The inclusive decay rate is measured by Mark III to be $(17.0 \pm 1.4) \times 10^{10}\mathrm{s}^{-1}$ [71]. Thus the modes not included here contribute only $(8 \pm 11)\%$ of the inclusive rate. This agrees with tight limits from explicit searches for higher modes such as $D \to K^*\pi\ell\nu$ [72]. The interpretation of this result is that the final state s quark from charm semileptonic decay is usually produced with a small enough momentum that it is bound in an $l = 0$ $q\bar{q}$ meson.

In summary, there has been a great deal of progress in measuring charm semileptonic decays. The form factor in $D \to \overline{K}\ell^+\nu$ is very well measured; the normalization agrees with lattice gauge calculations and quark models, and the shape agrees with the pole form. The decay rate for $D \to K^*\ell^+\nu$ is fairly well measured, and is lower than most predictions. We could use better form factor measurements to understand the comparison with theory better. These two decays saturate the total rate, at the present 10% level of the measurements.

Source		$f_+(0)$	$A_1(0)$	$V(0)$	$A_2(0)$
Exp	Ave	0.77 ± 0.04	0.61 ± 0.05	1.16 ± 0.16	0.45 ± 0.09
Quark Models	ISGW [4]	0.8	0.8	1.1	0.8
	WSB [65]	0.76	0.88	1.3	1.2
	KS [66]	0.7	0.82	0.8	0.8
	AW/GS [67]	0.7	0.8	1.5	0.6
Lattice Gauge	BKS [68]	0.76	0.83	1.4	0.6
	LMMS [69]	0.63	0.53	0.9	0.2
Sum Rules	BBD [70]	0.60	0.5	1.1	0.6

Table 18: Form Factors: Comparison with Theory

Mode	Source	$\Gamma(10^{10}\text{s}^{-1})$
$D \to \overline{K}\ell^+\nu$	D^0	8.9 ± 0.5
$D \to K^*\ell^+\nu$	$D^0 + D^+$	5.1 ± 0.5
$D \to \pi\ \ell\ \nu$	$D^0 + D^+$	1.2 ± 0.3
$D \to \rho\ \ell\ \nu$	theory	0.3 ± 0.1
Total		15.5 ± 0.8

Table 19: Summary of D Semileptonic Rates

4.6 Leptonic Decays and Decay Constants

I have already discussed the great interest in the decay constants of the heavy pseudoscalar mesons (f_D, f_B) for the study of mixing and CP violation. The theoretically expected range for f_B is from 140–270 MeV, which corresponds to a factor of 4 uncertainty in the decay or mixing rate. The best hope we have of narrowing this range with experimental data is to measure the charm decay constant. Then, using lattice gauge calculations or other techniqes, one can extrapolate to f_B. Naive scaling based on a simple picture of heavy meson wave functions predicts $f_B/f_D = \sqrt{m_d/m_b} = 0.6$. The lattice gauge caluculations find substantial corrections to this, getting values for this ratio in the range 0.8–0.9 [73, 74].

The value of f_D is expected to be in the range 170–300 MeV, with f_{D_S} about 10% larger. With values in this range, the branching ratios are expected to be $B(D^+ \to \mu^+\nu) = (2 - 7) \times 10^{-4}$ and $B(D_S^+ \to \mu^+\nu) = (3 - 9) \times 10^{-3}$. Mark III has placed an upper limit on the D^+ decay, $B(D^+ \to \mu^+\nu) < 7.2 \times 10^{-4}$, corresponding to a limit on the decay constant $f_D < 290$ MeV [75]. There is new information on the D_S^+ decay from two emulsion experiments and from CLEO.

The emulsion experiments are able to measure the D^+ direction with some accuracy before it decays. They use this to measure $p_{t\mu}$, the transverse momentum of the muon relative to the D^+ direction. The maximum value of muons from semileptonic decays is about 0.88 GeV/c, while the leptonic decays from the $D_S^+(D^+)$ give a Jacobian peak at 0.98(0.93) GeV/c. If the fake muons are small, the pure leptonic decay events should be visible beyond the endpoint in the $p_{t\mu}$ spectrum.

WA-75 has observed 6 events with $p_{t\mu} > 0.90$ GeV/c, with an estimated background, including from D^+ leptonic decays, of 0.8 [76]. Turning this into a branching ratio is somewhat difficult, since they observe no other D_s^+ modes cleanly. They measure the yield relative to inclusive semileptonic D^0 decays, with the result $\sigma B(D_s^+ \to \mu^+\nu)/\sigma B(D^0 \to X\ \mu^+\nu) = (1.25^{+0.55+0.24}_{-0.44-0.20}) \times 10^{-2}$. Using measurements of the D^0 and D_s^+ cross sections from NA-32 and the inclusive semileptonic branching ratio from Mark III, they calculate $B(D_s^+ \to \mu^+\nu) = (4.0^{+1.8+0.8}_{-1.0-0.6} \pm 1.7) \times 10^{-3}$, corresponding to $f_{D_S} = (232 \pm 45 \pm 20 \pm 48)$ MeV. The third error is the systematic error on the normalization.

E-653 is doing a similar analysis with a larger data sample. They have reported in a preliminary way an excess of events in the plot of p_t beyond the endpoint of the expected semileptonic spectrum. They are not ready to quote a branching ratio now, however. We look forward to this result in the near future.

CLEO-II has used a very different approach to observe $D_s^+ \to \mu^+\nu$, in which they observe the process $D_s^{*+} \to \gamma D_s^+, D_s^+ \to \mu^+\nu$ [77]. The missing momentum and energy in the hemisphere of the muon are used to estimate $\mathbf{p}_\nu$ and E_ν. For events in a broad $\mu\nu$ mass range around the D_s mass, the mass difference $\Delta M = M(\mu\nu\gamma) - M(\mu\nu)$ is plotted. Since the purely electronic decay is negligible, a similar spectrum for electrons serves as an ideal background sample. After taking into account differences in efficiencies and fake rates, they make the background-subtracted ΔM spectrum shown in fig. 4.6. There is a continuum from $D_s^+ \to \mu^+\nu$ combined with random gammas, and a peak at the expected mass from D_s^* decay. There are 39 ± 8 events in the peak.

CLEO measures the branching ratio for the leptonic decay relative to the benchmark $\phi\ \pi^+$ mode.The result is $\Gamma(D_s^+ \to \mu^+\nu)/\Gamma(D_s^+ \to \phi\ \pi^+) = 0.245 \pm 0.052 \pm 0.074$. They combine this with the value $B(D_s^+ \to \phi\ \pi^+) = (3.7 \pm 0.9)\%$ to measure the decay constant $f_{D_S} = 344 \pm 37 \pm 52 \pm 42$ MeV, where the last error is due to the uncertainty in the normalizing branching ratio. This result is at the upper end of the theoretical predictions, which center around 250 MeV. It is only 1 standard deviation from the WA-75 value, however. Clearly, this is an important number that needs to be measured more precisely.

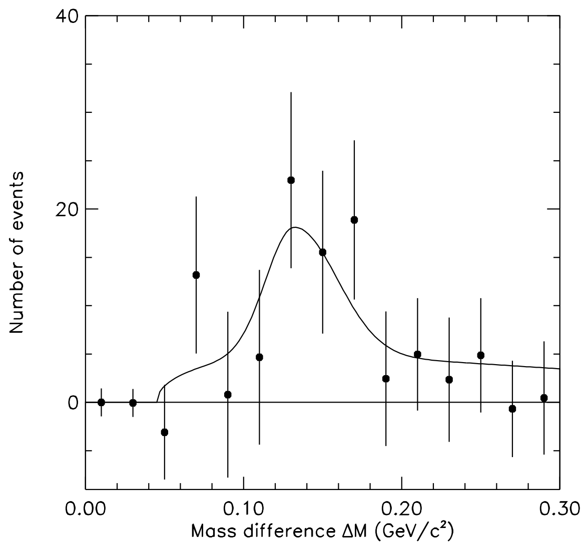

Figure 33: The ΔM spectrum from CLEO, showing evidence of the decay $D_s^+ \to \mu^+\nu$.

4.7 Conclusions on Charm Decays

1. The pattern of charm meson lifetimes can be understood fairly well with a simple model of spectator decays. Charm baryon lifetimes show the effect of additional spectator and non-spectator decays.

2. Simple models do not reproduce the individual hadronic branching ratios, however. This is partly due to large final state interactions, which have been measured for some modes.

3. The form factors for the dominant D semileptonic decays are fairly well measured. Much theoretical work is underway to understand these, and to gain what understanding we can about $b \to u$ exclusive semileptonic decays.

4. The scale of absolute branching fractions has been measured very accurately for the D^0, somewhat less so for the D^+.

5. There is evidence of the leptonic decay $D_s \to \mu^+\nu$. We will soon have a few measurements of f_{D_s}.

The leading new results in charm decays are either detailed measurements of important quantities (semileptonic form factors) or discoveries of very rare processes (DCSD, leptonic decays). Studies of $D^0 - \overline{D}^0$ mixing, f_{D_s}, and $D \to K^*\ell\nu$ form factors should have high priority with new, larger data samples.

5 CHARM SPECTROSCOPY

Although most of these lectures are concerned with the weak decays of charm and bottom mesons, in this section I will discuss the spectroscopy of $c\overline{q}$ mesons. In general, heavy quark-light quark mesons provide a test of our knowledge of QCD at low momentum. Precise measurements of the $L = 1$ $c\overline{q}$ mesons now exist, and provide the first experimental test of theoretical ideas.

The spin-parity assignments expected for the lowest-lying mesons are shown in table 20. The experimental information consists of mass splittings and decay widths. The spin-parity assignments are made mostly on the basis of decay modes, although some times angular distributions are useful.

L	J^P
0	$0^-,\ 1^-$
1	$0^+,\ 1^+,\ 1^+,\ 2^+$

Table 20: The spin-parity assignments of the lowest-lying charm mesons.

Heavy Quark Effective Theory makes predictions on the properties of heavy mesons:

1. The mass splittings and widths are independent of flavor, and can be scaled with the mass of the heavy quark.
2. Each spectroscopic line consists of a doublet with $J_{\pm} = j \pm 1/2$, where j is the vector sum of the orbital angular momentum and the spin of the light degrees of freedom.
3. The ratios of partial widths are also predicted.

5.1 L=0 Charm Mesons

The best known and studied charm mesons have the charm quark and light antiquark in an L=0 bound state. The masses of the mesons are shown in table 21. In all cases, $\Delta M = M(1^-) - M(0^-) \approx 142$ MeV. The fact that this is so close to the pion mass leads to a large isospin "violation" in the production of D mesons. The D^{*+} decays into both D^0 and D^+; the D^{*0} decays into D^0 only, because the $D^+\pi^-$ state is forbidden. That leads to the typical production ratio, $N(D^0) \approx 2N(D^+)$.

The mass splitting is due to the difference in energy between the parallel and antiparallel spins. As we saw in Howard Georgi's lectures at this school, in a quark model we expect this splitting to scale like $1/m_Q m_q$, using the constituent quark masses. The $K^* - K$ splitting is about 400 MeV, and the

$^{2S+1}L_J$	J^P	$c\overline{u}$	$c\overline{d}$	$c\overline{s}$
$^1S_0$	0^-	1865	1869	1969
$^3S_1$	1^-	2007	2010	2110

Table 21: The masses of the L=0 charm mesons

$D^* - D$ splitting is 140 MeV, which are in the rough ratio of the m_c/m_s. If we scale this up to the b quark system, this corresponds to a $B^* - B$ splitting of about 45 MeV, which agrees very well with the measured value of 46 MeV. The fact that in the $c\overline{s}$ system the measured splitting is also about 140 MeV is not obvious; it depends on the fact that $\frac{|\psi(0)|^2}{m_q}$ happens to be the same for strange and light antiquarks.

5.2 L=1 Charm Mesons

There are four L=1 charm mesons, as shown in table 20. The most useful attribute in making spin-parity assignments is the dominant decay mode. The 0^+ D_0^* mesons decay into $D\pi$ with an s-wave; the two 1^+ D_1 mesons decay into $D^*\pi$ in either s-or d-wave; and the 2^+ D_2^* meson decays into both modes with a d-wave.

There are two possible patterns of grouping the four mesons into multiplets. The grouping known well from charmonium is a division by the total spin S: a triplet with $S = 1$ and a singlet with $S = 0$. Of course in charmonium, these two multiplets have different C parity. The D mesons are not C eigenstates, however, so S may not be a relevant quantum number.

The other pattern possible is to group the four states into two doublets: one with $j = 3/2$ and one with $j = 1/2$. The $j = 3/2$ doublet would include the 2^+ and one 1^+ state; the $j = 1/2$ doublet would include the 0^+ and the other 1^+ state. So the question is whether the proper quantum number is S or j. In general, of course, the actual states may represent some linear combinations of these two pictures. The two 1^+ mesons may be eigenstates of neither S or j.

HQET gives us some guidance on this point. In the $M_Q >> \Lambda_{QCD}$ limit, the scheme of two doublets is preferred. According to HQET [82], the wave functions of the light constituents does not depend on the flavor or spin of the heavy quark. In particular, HQET predicts a doublet with $j = 3/2$ which decays in d-wave, and a doublet with $j = 1/2$ which decays in s-wave. The connection between j and the final state angular momentum is straightforward once one assumes that the heavy quark spin decouples. Because of the extra factor of p^4 for the d-wave decay rate and the low momentum in the decay the $j = 3/2$ states are expected to be much narrower than the $j = 1/2$ states [83].

The data on charm spectroscopy come from fixed target experiments and from e^+e^- experiments in the upsilon region. The easiest decay to observe is $D_1^0 \to D^{*+}\pi^-$, because of the clean D^{*+} signal. The absence of a signal in the $D^+\pi^-$ mode identifies this as a probable $J^P = 1^+$ state. Figure 34 shows the $D_2 \to D\pi$ signals from E-687 [84]. These states are more difficult to see because they require clean D^+ and D^0 peaks to start with. CLEO observes the decay $D_2^{*0} \to D^{*+}\pi^-$, with a branching ratio about 1/2 that for the $D^+\pi^-$ decay. This ratio is consistent with the $J^P = 2^+$ assignment. The masses and widths for these mesons are shown in table 22.

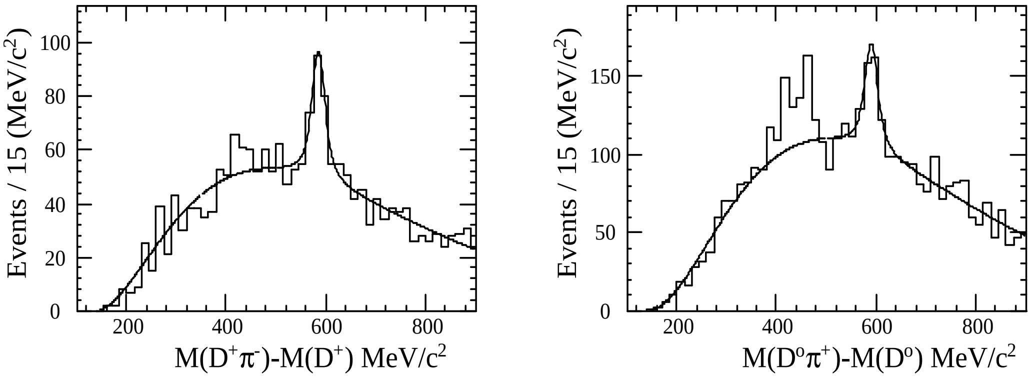

Figure 34: The mass plots for the decays $D_2^{*0} \to D^+\pi^-$ (left) and $D_2^{*+} \to D^0\pi^+$ (right) from E-687. The lower peak in the $D^0\pi^+$ plot is from the decay $D_1^{*0} \to D^{*0}\pi^+$ where only the π^0 or γ from the D^{*0} decay is not observed.

J^P	$c\overline{u}$	$c\overline{d}$	$c\overline{s}$
2^+ M	2457.7 ± 1.9	2456 ± 6	2573.2 ± 1.9[85]
Γ	21 ± 5	23 ± 10	16 ± 6
1^+ M	2422.8 ± 3.2		2535.35 ± 0.34
Γ	18^{+6}_{-4}		< 2.3

Table 22: The masses and widths of the observed $L = 1$ mesons, in MeV. The values are taken from the Review of Particle Properties except for the D_{s2}^+.

The excited D_s mesons have been discovered more recently. The decay $D_s^* \to D_s^{(*)}\pi$ is forbidden by isospin. Thus the dominant decays are $D_{s1}^+ \to D^*K$ and $D_{s2} \to DK$. Figure 35 shows the mass peaks for $D_{s1}^+ \to D^{*0}K^+$ and $D_{s1}^+ \to D^{*+}K_S^0$. Because the energy released in the decay is small, the resolution is quite good and the backgrounds relatively small. The most recent addition to the list of observed charm mesons is the D_{s2}, seen by CLEO [85] in the decay mode D^0K^+. The masses and widths of the L=1 D_s mesons are shown in table 22.

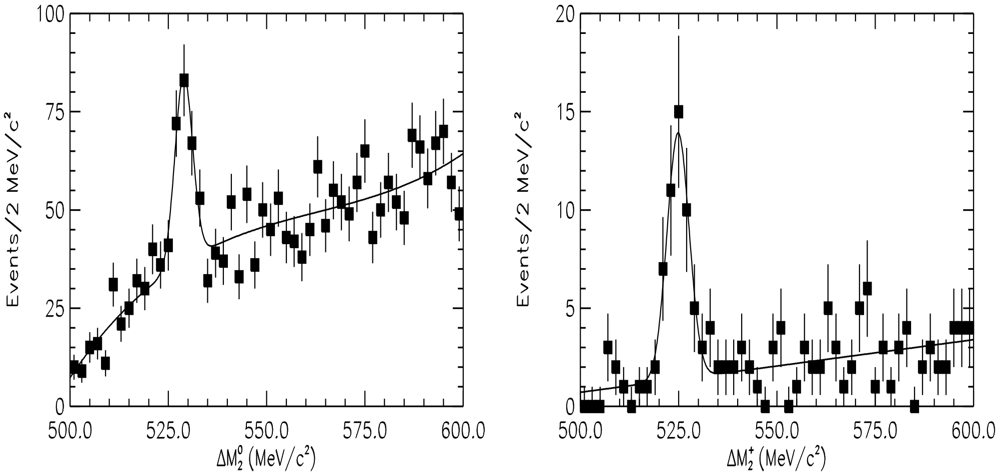

Figure 35: The mass plots for the decays $D_{s1}^+ \to D^{*0}K^+$ and $D_{s1} \to D^{*+}K_S^0$ from CLEO.

The most important feature of the table is that for each $c\overline{q}$ combination only the 2^+ and at most one 1^+ state has been observed, with a mass splitting of about 37 MeV. The widths are less than about 25 MeV, which is a small value for a mass difference of about 500 MeV. These facts are consistent with the HQET picture of a $j = 3/2$ doublet with narrow width. Presumably the two states which decay by s-wave are much wider, and may take a partial wave analysis with high statistics to observe, as was needed for the excited K mesons.

6 CP VIOLATION IN B DECAY

6.1 The Standard Model Predictions

To observe the CP-violating phase in the CKM matrix, we need to have interference between two decay amplitudes which have a relative weak phase. To get a large asymmetry, the two amplitudes should be of comparable size. For the decays of the B^0 into CP eigenstates ($\pi^+\pi^-$, ψK_S^0), mixing provides this interference. Moreover, the size of the asymmetry is completely determined by the CKM matrix elements, in the limit that the single spectator diagram dominates the decay process.

This technique also works well for two separate cases in which the final states are not CP eigenstates. One case is a self-conjugate final state which can exist in a mixture of partial waves with different CP parities. An important example of this is $B^0 \to \psi K^{*0}$. One can separate the CP-eigenstates by cuts on the angular distributions, although in this specific case there is evidence that one partial wave dominates.

The other case is a final state that is not self-conjugate at the particle level, but is at the quark level, such as $B^0 \to \rho^\pm\pi^\mp$. As long as the two decay modes have comparable branching ratios, the interference will lead to large asymmetries, as for CP eigenstates. And since the modes are dominated by the same diagrams, the CKM phases are equal and opposite, as in the CP eigenstate case. I will use the phrase "CP final state" in what follows to denote either the CP eigenstate, or one of these other two types of final states useful for CP studies.

We can take the discussion of mixing from section 2 and relax the requirement of CP symmetry. Allowing for CP violation, the two mass eigenstates of the B^0 can be rewritten

$$\begin{aligned} |B_L\rangle &= p|B^0\rangle + q|\overline{B}^0\rangle \\ |B_H\rangle &= p|B^0\rangle - q|\overline{B}^0\rangle \end{aligned} \tag{30}$$

where $q = e^{i\phi_M}/\sqrt{2}$ and $p = e^{-i\phi_M}/\sqrt{2}$. The ratio of the two amplitudes is just a phase rotation,

$$q/p = (V_{tb}^* V_{td})/(V_{tb} V_{td}^*) = e^{2i\phi_M}. \tag{31}$$

The amplitudes for decays into a given CP final state f_{CP} are $A(\overline{A})$ for $B^0(\overline{B}^0) \to f_{CP}$. When only a single amplitude with a given weak decay phase ϕ_D dominates the decay, the ratio $\overline{A}/A = e^{-2\phi_D}$. The two processes that interfere are $B^0 \to f_{CP}$ and $B^0 \to \overline{B}^0 \to f_{CP}$. Thus there are two separate phases which contribute to the relative phase of the two paths, ϕ_M and ϕ_D.

Defining

$$r(f) \equiv \frac{q}{p}\frac{\overline{A}}{A} = e^{2i(\phi_M - \phi_D)}, \tag{32}$$

one can then write the time dependent rates for initially pure states as

$$\Gamma(B^0(t) \to f) \propto |A|^2 e^{-\Gamma t} \times \Big(1 \pm \text{Im } r \ \sin(\Delta m t)\Big). \tag{33}$$

Here the lower sign corresponds to an initial $\overline{B}^0$. Defining the time dependent CP asymmetry

$$a_f(t) \equiv \frac{N(B^0(t) \to f) - N(\overline{B}^0(t) \to f)}{N(B^0(t) \to f) + N(\overline{B}^0(t) \to f)}, \tag{34}$$

and plugging in equations 32 and 33, the asymmetry can be expressed

$$a_f(t) = 2 \ \text{Im}(r)\sin(\Delta m t) = -\sin[2(\phi_M - \phi_D)]\sin(\Delta m t). \tag{35}$$

Thus the asymmetry is oscillatory, with an amplitude $-\sin[2(\phi_M - \phi_D)]$. Because $x_d = \Delta m/\tau \approx 0.65$, the asymmetry reaches its maximum absolute value at a time $t \approx 2.3 \ \tau_{B^0}$.

What are the values of ϕ_M and ϕ_D? The value of ϕ_M is obtained by evaluating the argument of the amplitude for the mixing diagram, which is just the argument of V_{td} in the Wolfenstein parameterization. The value of ϕ_D depends on the quarks involved in the spectator decay diagram. Table 23 shows the values of $\phi_M - \phi_D$ for decays of interest.

Decay	Example	$\phi_M - \phi_D$
$b \to c\bar{c}s$	ψK^0_S	β
$b \to c\bar{c}d$	D^+D^-	β
$b \to u\bar{u}d$	$\pi^+\pi^-$	α
$b \to s\bar{s}d$	$\phi\pi^0$	0

Table 23: The phases that determine the amplitude of the CP asymmetry for several B^0 decay modes.

Thus, the time dependent asymmetry for an initial B^0 decaying into ψK^0_S is $a_f(t) = -\sin(2\beta)\sin(\Delta M t)$. Using the center of the allowed region, one would have $\sin(2\beta) \approx 0.6$, which gives a very large asymmetry. The limits on $\sin(2\beta)$ from figure 13 are (0.25–0.90). Clearly this will be the first CP asymmetry seen, if the Standard Model is correct. The range for $\sin(2\alpha)$ is (-0.7–1.0). Measuring $\sin(2\gamma)$ in this way involves studying time dependence of asymmetries in B_s decays, which is extremely difficult because of the short mixing time. That will probably be the last CP parameter to be measured.

The identification of a decay mode with a CKM phase depends on the fact that there is a single quark diagram which is dominating the final state. This is almost certainly a good assumption for decays such as $B^0 \to \psi K^0_s$ and $B^0 \to D^+D^-$. It is not so clear for the decays that will be used to measure $\sin(2\alpha)$, however, such as $B^0 \to \pi^+\pi^-$, where the amplitude for the spectator decay may only be somewhat larger than the Cabibbo-suppressed version of the penguin-diagram decay that is responsible for $B^0 \to K^+\pi^-$

This so-called "penguin pollution" does not make it impossible to measure the CKM angle well. The penguin amplitude will probably be smaller than the spectator amplitude by a factor of around 5. Second, it is possible to use the other $B \to \pi\pi$ decays to extract the CKM phase from the measured asymmetry [86]. It might cause some reduction in the sensitivity relative to the case of a completely dominant spectator decay, however.

6.2 Measuring CP Asymmetries at the $\Upsilon(4S)$.

The reasons to do the CP measurement at the $\Upsilon(4S)$ are the reasons why taking data there has been so successful for B physics in the past.

1. The $B^0\overline{B}^0$ cross section is large ($\sigma = 0.5$ nb).
2. There are no additional fragmentation hadrons.
3. The B^0 is almost at rest in $\Upsilon(4S)$ rest frame.
4. The $B^0/\overline{B}^0$ pair will remain in a $B^0/\overline{B}^0$ state (even though each meson may mix into the opposite flavor) until one decays.

The strategy is to select events in which one B decays to a CP final state and the other produces a unique tag of B^0 or $\overline{B}^0$ decay. The tag is provided most readily by using a hard lepton from $\overline{B}^0 \to X_c\ell^-\nu$, or a charged kaon from $X_c \to K^-X$.

The time that governs the evolution of the CP violation is $t_2 - t_1$, where t_1 is the proper time at which one B decays into a tagging mode and time t_2 is the proper time at which the other B (which must be of opposite flavor if $t_2 = t_1$) decays into a CP final state. Then the doubly differential decay rate is

$$\frac{dN}{dt_1 dt_2} \propto e^{-(t_1+t_2)/\tau}[1 \pm \sin(2\beta)\sin(x(t_2 - t_1)/\tau)] \tag{36}$$

The two signs correspond to the tagged particle being a B^0 or $\overline{B}^0$. Note that if one integrates over both times the asymmetry integrates to zero! That is why the relative decay time must be measured.

Figure 36 demonstrates the size of the CP asymmetry expected. It shows the distribution in $t = t_2 - t_1$ for decays into ψK^0_s starting with a tagged

$B^0(\overline{B}^0)$ state at $t = 0$. I have used for the mixing parameter $x_d = 0.65$ and for the CP asymmetry $\sin(2\beta) = 0.6$, which is near the middle of the allowed range. One can see that the asymmetries are quite large, and that they approach the maximum value within the first lifetime.

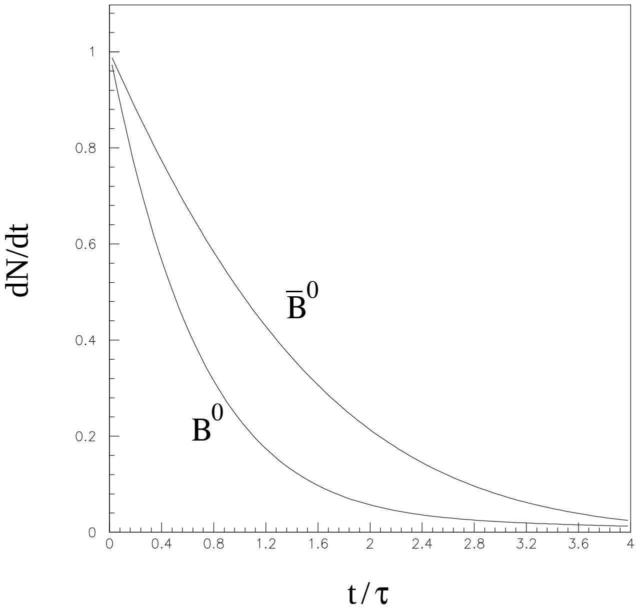

Figure 36: The time dependence of the decay rate into ψK_s^0 for a tagged $B^0(\overline{B}^0)$. At the $\Upsilon(4S)$ the time variable is $t = t_2 - t_1$, where t_1 is the proper time at which the tagging B decays and t_2 is the proper time at which the other B decays into the CP final state. For $t < 0$, the B^0 and $\overline{B}^0$ plots are reversed.

There are two experimental requirements for making decisive measurements of the CP asymmetries at the $\Upsilon(4S)$: (1) an unprecedented luminosity of $3 \times 10^{33}\mathrm{cm}^{-2}\mathrm{s}^{-1}$ and (2) measurement of the relative decay time $t_2 - t_1$. These are the two requirements that lead to the basic design of the SLAC and KEK B-factories. They are two ring machines, which make it possible to achieve bunch spacings of about 4 nsec, increasing the luminosity. In addition, the two rings operate at different energies, such as 3.1 GeV on 9.0 GeV. This gives the produced Bs a boost in the laboratory, which makes it possible to measure the relative lifetime.

The first question that was asked when people took a serious look at asymmetric B factories was whether one could measure the decay time well enough. For the case of 3.1×9.0 GeV, the average separation between the two decay vertices is about 250 μm, using a B lifetime of 1.54 nsec. Studies have shown that with a beam pipe radius of 2.5 cm, the resolution in the separation between the two B decay vertices is around 80 μm. (There are tails on the distribution which makes it somewhat difficult to quote a single number.) Using these numbers, one finds negligible degradation of the asymmetry measurement compared to perfect vertex resolution. Moreover, since this resolution is determined by multiple scattering and not intrinsic resolution of the detector, it should be a reliable estimate.

CLEO-II is a prototype for a B-factory detector [87]. Its excellent momentum resolution for charged tracks and detection efficiency and energy resolution for low momentum γs are needed to do well at the $\Upsilon(4S)$. In addition, there are a number of major improvements and additions necessary for a B-factory detector. The improvements needed are:

1. a drift chamber with He-based gas to reduce multiple scattering,
2. reduced amount of material before the CsI in the forward endcap,
3. a higher rate capability for all detector components, and
4. larger acceptance at forward angles.

The needed additions are:

1. a silicon vertex detector with good z resolution,
2. a Cerenkov-based hadron identification device to separate $B^0 \to \pi^+\pi^-$ from $B^0 \to K^+\pi^-$, and
3. (optional) instrumented flux return to lower the threshold for useful muons.

These are the basic design requirements for the BABAR experiment at PEP-II [88] and for the BELLE experiment at the KEK B-factory [89]. In addition, they are pretty much the same requirements for the CLEO-III upgrade now being developed [90]. So there is a large world-wide effort in developing the detectors needed to satisfy these requirements.

6.3 Sensitivity to CP Asymmetries

One expects that by the time that the CP asymmetries in B^0 decay are measured, the CKM unitarity triangle will be significantly better known than it is today. There should be more precise measurements of m_t and V_{cb}, for example. Better measurements of the inclusive decay $B \to X_u \ell\nu$ and first measurements of exclusive decays such as $B \to \rho(\omega)\ell\nu$ should improve our knowledge of $|V_{ub}/V_{cb}|$. Various calculations of the hadronic matrix element in K^0 mixing should agree, and lower the systematic error on extracting the CKM constraint from ϵ.

There are also a number of approaches that may improve the determination of $|V_{td}|$. One of these is to use B_d mixing as we do know, but with a better calculation of f_B. Another is to measure B_S mixing, which makes it possible to use the ratio x_d/x_s to determine the ratio of CKM elements with little hadronic complication. A third approach is to measure the rare decay $K^+ \to \pi^+\nu\overline{\nu}$, which again should give V_{td} with little theoretical error. At least one of these approaches should lead to some success over the next few years.

Thus there will be much progress in these measurements and calculations over the next four years, by the time the B-factories turn on. In addition, the B-factories and other experiments will contribute further to improving our information after that. Consider the status in the year 2001, a time by which one should have fully analyzed data from a long run at full luminosity from the two asymmetric B-factories. Figure 37 shows a plausible version of what the status of the unitarity constraints might be around the year 2001, not including those from CP asymmetry measurements in B decays. In setting the widths of the bands, I assume some reasonable amount of progress, both theoretical and experimental, due to the enormous amount of effort on determining these parameters. The central values are chosen totally arbitrarily, of course.

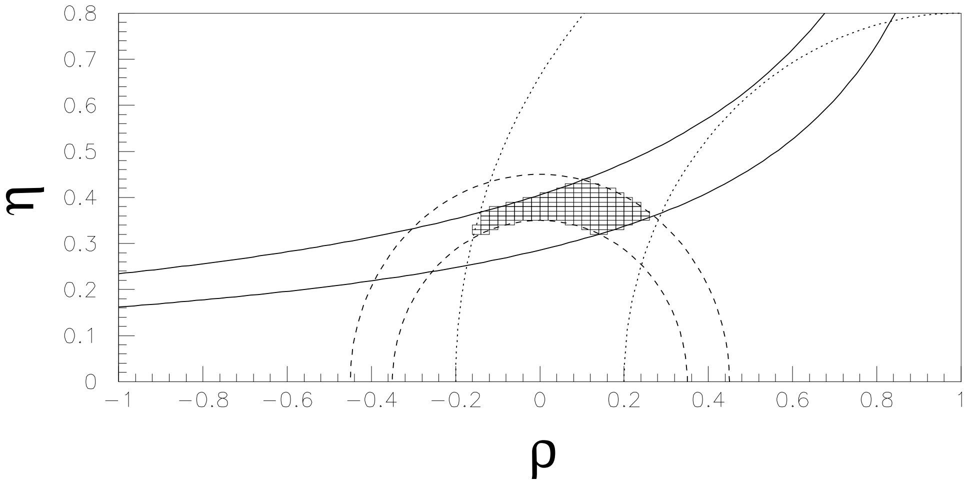

Figure 37: An example of what the unitarity triangle might look like seven years from now, without constraints from CP asymmetries in B decay. The allowed region for the CKM parameters ρ and η is shaded. The central values of the bands are, of course, arbitrary.

The sensitivity to the CP violation in B^0 decays is set by the following parameters (The efficiencies are taken from the BABAR Letter of Intent [88], and are obviously preliminary estimates.):

- N, the number of $B^0\overline{B}^0$ events, which for a luminosity of $3\times10^{33}\mathrm{cm}^{-2}\mathrm{s}^{-1}$

and 2 years of running is $N = 6 \times 10^7$.

- B, the branching ratio for the CP mode. For ψK_S^0, $\psi \to \ell^+\ell^-$, this is about 5×10^{-5}.
- ϵ_c, the efficiency for observing the decay $B \to f_{CP}$. For ψK_S^0, $\epsilon_c = 0.47$.
- ϵ_t, the effective tagging fraction. $\epsilon_t = \epsilon_{tag}(1-2w)^2 = 0.36$.
- d, a dilution factor to take into account the ratio between the average asymmetry and the maximum value. This is about 0.5, close to the value for perfect vertex resolution.

From these, one can estimate the error in $\sin(2\beta)$:

$$\delta[\sin(2\beta)] = \left[N\epsilon_c\epsilon_t d^2\right]^{-1/2}. \quad (37)$$

For example, for $B \to \psi K_S^0$, this gives $\delta[\sin(2\beta)] = 0.09$.

Including a few modes, the expected errors are $\delta[\sin(2\beta)] = 0.06$ and $\delta[\sin(2\alpha)] = 0.08$. The error on $\sin(2\alpha)$ is based on expected measurements of the modes $B^0 \to \pi^+\pi^-$ and $B^0 \to \rho^\pm\pi^\mp$, and is therefore quite uncertain. If one were to achieve such measurements, one would get constraints on the unitarity triangle as shown in figure 38. The measurements would overconstrain the unitarity triangle, and would constitute an extremely powerful test of the Standard Model explanation of CP violation.

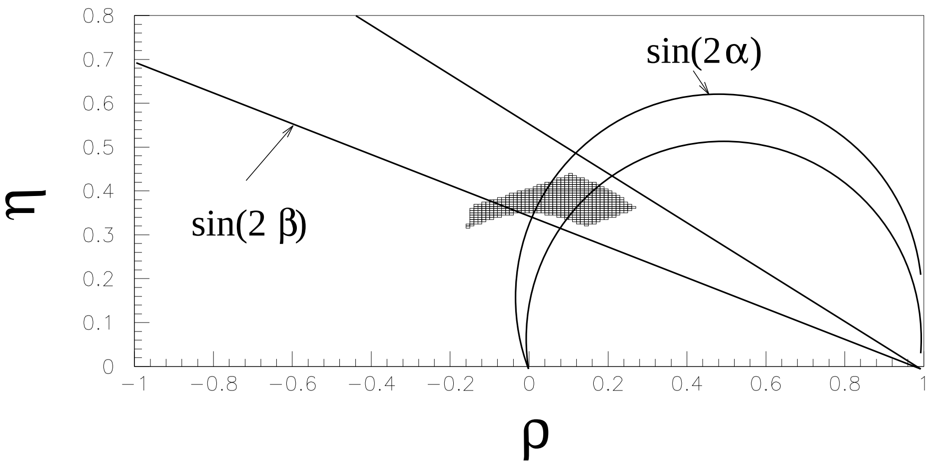

Figure 38: An example of what the constraints on the unitarity triangle should be from the measurements of CP asymmetries described in the text. The shaded region is the same as in the previous figure. The central values of the bands are, of course, arbitrary.

There are two possible outcomes to this experiment, and each one has important consequences. If after some period of time, one sees a result as shown in figure 38, then one has overwhelming experimental evidence that all of the observed CP violating effects are due primarily to the CKM phase. More precise measurements and comparisons among modes will be required to see if there is evidence of a smaller contribution from nonstandard sources. In addition, one would try to use the precise measurements of quark masses and mixing angles to discover their underlying source.

If the CP violation in K_L decay is not from the CKM phase, on the other hand, the measured asymmetries could take any value. In some models one would get asymmetry amplitudes close to zero rather than about 0.6. In others, one would get large asymmetries but ones that would not satisfy the constraint of closing the unitary triangle. (This is not a failure of unitarity, of course, but simply evidence that we are misinterpreting a measurement, for example because the CP violation in K_L decay is due to physics outside the Standard Model.) We would then have hard evidence of new physics. The extreme sensitivity of mixing and CP violation to new physics means that this is a very good place to search for such new phenomena.

6.4 CP Violation in B Decays at Hadron Machines

We have seen that CDF already has a large, clear signal for $B^0 \to \psi K_s^0$. For about 10 years now, people have been studying the prospects for studying CP violation in B^0 decays at hadron colliders. The immediate interest, of course, is at the Tevatron with the Main Collider upgrade.

The B production rate is extremely high. Recent measurements show cross sections agreeing with next-to-leading-order calculations of a few μb. The mode $B^0 \to \psi K_s^0$ is perfect for the hadron collider experiments because the $\psi \to \mu^+\mu^-$ decay is easy to trigger on and very clean. One experimental issue will be to trigger efficiently on low momentum ψs at an order of magnitude more luminosity. Triggering on other modes of interest for CP studies, such as D^+D^- and $\rho^+\pi^-$ is harder; techniques to do this are not yet tested by the existing experiments.

For the ψK_s^0 experiment at a hadron collider, the greatest uncertainty is probably in the effective tagging efficiency. Lepton tagging should work well at large p_t. At somewhat lower p_t, there is a trade-off between higher efficiency and wrong-sign tags due to secondary leptons. Kaon tagging is harder, even if hadron identification devices are added, because most of the tagging kaons are around 1 GeV/c in momentum, where there are many other kaons around. Other possible tagging schemes involve observing decays of excited B mesons, and using the charge of nearby fragmentation pions. In all tagging schemes not using leptons, the difficult challenge is to lower the wrong sign fraction to around 10–15%, so that they add appreciably to the effective tagging efficiency.

The present run of CDF and D0 will provide important engineering information for future B experiments at the Tevatron. For example, the tagging efficiencies and wrong sign fractions for various techniques can be measured well using modes such as $B^- \to \psi K^-$. Both experiments are upgrading for Main Injector running at five times the luminosity of the present run. There are further upgrade proposals for future running, and new proposals explicitly designed for B physics at the Tevatron. There will also be a proposal for B physics at LHC. There the higher energy provides a higher fraction of events with $b\bar{b}$ production. The higher LHC luminosity, although crucial for the Higgs physics that drives the accelerator design, may well not be useful for experiments operating at relatively low p_t.

HERA-B is an experiment which will use the halo of the 800-GeV proton beam from HERA colliding with a wire target. The duty cycle is likely to be significantly better than extracted proton beams. In other respects, the experimental environment is very much like fixed target at FNAL. The main concerns are therefore the same: (1) what is the highest interaction rate at which the trigger and tracking are efficient? and (2) how efficiently can one tag the other B? The experiment has been given preliminary approval. It should be ready for an engineering–cross section run in 1996.

6.5 Measuring CP Violation without Mixing

The above discussion considered CP asymmetries in B^0 decays in which mixing provides the alternative path to the final state. The primary advantages of measuring the CP asymmetries in these modes are that they are known to be large, as we have seen, and that the size of the asymmetry is directly related to CKM matrix elements, without complications of hadronic matrix elements.

There are other ways one could possibly see CP violation in B decays. These all involve using interference between two diagrams, neither of which is mixing. The difficulty is finding decays in which the two interfering amplitudes are of similar size. The effects are likely to be extremely hard to observe, but it is important to look for the unexpected. The main differences experimentally are that the asymmetries are not time-dependent, so there is no advantage to measuring the time evolution, and they can be measured in self-tagging decays, so tagging the flavor of the other B is unnecessary. One may need to measure time-dependent asymmetries to extract information on CKM phases, however.

As an example, the decays $B^+ \to K^0\pi^+$, $B^+ \to K^+\pi^0$, $B^0 \to K^+\pi^-$, and $B^0 \to K^0\pi^0$ together represent an interesting place to look. As I discussed earlier, there is a penguin-diagram decay $b \to sq\bar{q}$ which probably dominates, but there is also the suppressed spectator decay $b \to us\bar{u}$. The penguin decay only populates the $I = 1/2$ final state, while the spectator decay leads to both $I = 1/2$ and $I = 3/2$. If good measurements are available for all four modes, it is possible to untangle the weak and strong phases. Of course, if one could measure an asymmetry, that would be very interesting even if one had not assembled all of the information to relate it to a CKM phase.

The CLEO results on $B^0 \to K^+\pi^-$ and $B^0 \to \pi^+\pi^-$ demonstrate the difficulty of observing these rare B decay modes. Efficiencies for the other three $B \to K\pi$ modes are significantly lower, and the backgrounds higher. Clearly higher luminosities are needed, and probably the ultraclean environment of the $\Upsilon(4S)$ are needed to do CP studies using such modes. These will be high priority physics goals for the CLEO-III upgrade and for the two B-factories.

6.6 Conclusions

After studying all of the material that was needed to prepare these lectures, I was left with one primary conclusion. Our understanding of the weak decays of heavy quarks has gone through a revolution in the last ten years. We have a detailed theoretical framework in which we can understand many of the experimental features. As a result of this understanding, we can predict the existence of large asymmetries in B^0 decays with some degree of confidence, unless the Standard Model does not explain the familiar CP violation observed in K_L decays.

For the next five years, the program is clear:

1. Improve our knowledge of the CKM matrix with better measurements of $|V_{ub}|$, $V_{cb}|$, and f_{D_s}, together with better calculations of decay constants and form factors.

2. Measure the branching ratios for rare modes important for CP studies: $B^0 \to \pi^+\pi^-$, $\rho^+\pi^-$, and $K^+\pi^-$.

3. Look for something unexpected, such as anomalous CP violation in B^- decay or large D^0 mixing.

In five years or so, we start what will probably be the final stage of the now thirty-year old search for the source of CP violation. There will be a number of precise measurements that will overconstrain the unitarity triangle. We will learn whether the CP violation we have observed is described in the Standard Model, or lies totally outside it. And in either case, we will be one step closer to understanding what more fundamental theory lies underneath our present picture. It will be a very interesting time.

7 ACKNOWLEDGMENTS

In preparing these lectures I have benefited from discussions with my colleagues at UCSB, especially Rolly Morrison, Harry Nelson, and Jeff Richman. In the area of semileptonic decays, I have lifted ideas, figures, and bits of text from the reviews by Morrison and Richman for the Particle Data Book and by Richman and Pat Burchat for Reviews of Modern Physics. I have also been helped by many CLEO colleagues who provided figures. Finally, I must acknowledge Tom Ferbel, who required that I write up the lectures.

References

[1] N. Isgur and M.B. Wise, Phys. Rev. D**42**, 2388 (1989).

[2] J. Bartelt *et al.* (CLEO), *Inclusive Measurement of B-Meson Semileptonic Branching Fractions*, submitted to the XVI International Symposium on Lepton and Photon Interactions, Ithaca, New York (1993).

[3] G. Altarelli, N. Cabibbo, G. Corbò, L. Maiani, and G. Martinelli, Nucl. Phys. B **208**, 365 (1982).

[4] N. Isgur, D. Scora, B. Grinstein, and M. Wise, Phys. Rev. D **39**, 799 (1989).

[5] H. Albrecht *et al.* (ARGUS), Phys. Lett. B **249**, 359 (1990).

[6] H. Albrecht *et al.* (ARGUS), Phys. Lett. B **318**, 397 (1993).

[7] J. Gronberg *et al.* (CLEO), CLEO conference paper CLEO CONF 94-6, submitted to the Glasgow conference ICHEP94 (1994).

[8] W. Venus, *b Weak Interaction Physics in High Energy Experiments*, in AIP Conference Proceedings 302, Lepton and Photon Interactons, XVI International Symposium, eds. P. Drell and D. Rubin, Ithaca, NY (1993), p. 2

[9] Particle Data Group, *Review of Particle Properties*, Phys. Rev. **D50**, 1173(1994).

[10] M. Shifman, N.G. Uraltsev, and A. Vainshtein, Minnesota preprint TPI-MINN-94/13-T and hep-ph/9405207 (1994).

[11] B. Barish *et al.* (CLEO), CLEO preprint CLNS 94/1285 (1994).

[12] H. Albrecht *et al.* (ARGUS), Z. Phys. C **57**, 533 (1993).

[13] M. E. Luke, Phys. Lett. B **252**, 447 (1990).

[14] M. Neubert, CERN Report CERN-TH.7395/94 and hep-ph/9408290 (1994), submitted to Phys. Lett. B.

[15] T. Mannel, CERN Report CERN-TH.7162/94 (unpublished).

[16] H. Albrecht *et al.* (ARGUS), Phys. Lett. B **324**, 249 (1994).

[17] H. Albrecht *et al.* (ARGUS), Z. Phys. C **57**, 533 (1993).

[18] H. Albrecht *et al.* (ARGUS), Phys. Lett. B **234**, 409 (1990).

[19] R. Fulton *et al.* (CLEO), Phys. Rev. Lett. **64**, 16 (1990).

[20] J. Bartelt *et al.* (CLEO), Phys. Rev. Lett. **71**, 4111 (1993).

[21] J. Bartelt *et al.* (CLEO), Phys. Rev. Lett. **71**, 1680 (1993).

[22] H. Albrecht *et al.* (ARGUS), Z. Phys. **C55**, 357 (1992).

[23] H. Albrecht *et al.* (ARGUS), Phys. Lett. **B324**, 249 (1994).

[24] A.J. Buras, M.E. Lautenbacher, and G. Ostermaier, MPI-München preprint MPI-Ph/94-14 and HEP-PH-9403384 (1994).

[25] D. Buskulic *et al.* (ALEPH), Phys. Lett. **B314**, 459 (1993).

[26] P.D. Acton *et al.* (OPAL), Z. Phys. **C60**, 217 (1993).

[27] O. Adriani *et al.* (L3), Phys. Lett. **B317**, 474 (1993).

[28] P. Abreu *et al.* (DELPHI), Z. Phys. **C63**, to appear (1994).

[29] F. Abe *et al.* (CDF), Phys. Rev. Lett. **71**, 3421 (1993).

[30] P. Abreu *et al.* (DELPHI), Phys. Lett. **B312**, 253 (1993).

[31] P.D. Acton *et al.* (OPAL), Phys. Lett. **B307**, 247 (1993).

[32] D. Buskulic *et al.* (ALEPH), Phys. Lett. **B307**, 194 (1993).

[33] P. Abreu *et al.* (DELPHI), Z. Phys. **C57**, 181 (1993).

[34] K. Abe *et al.* (CDF), Phys. Rev. Lett. **72**, 3456 (1994).

[35] M. Athanas *et al.* (CLEO), Cornell preprint CLNS94/1286 (1994).

[36] H. Albrecht *et al.* (ARGUS), Phys. Lett. **B275**, 195 (1992).

[37] H. Albrecht *et al.* (ARGUS), Phys. Lett. **B232**, 554 (1989).

[38] M. Neubert, *Heavy Quark Symmetry*, SLAC–PUB–6263, June 1993, to appear in Physics Reports.

[39] J. Gronberg *et al.* (CLEO), CLEO conference paper CLEO CONF 94-7.

[40] F.J. Gilman and R.L. Singleton, Jr., Phys. Rev. **D41**, 93 (1990).

[41] J.G. Körner and G.A. Schuler, Z. Phys. **C46**, 93 (1990).

[42] S. P. Booth *et al.* (UKQCD), Phys. Rev. Lett. **72**, 462 (1994).

[43] C. Bernard, Y. Shen, and A. Soni, Phys. Lett. B **317**, 164 (1993).

[44] J. Mandula and M. Ogilvie, Nucl. Phys. B (Proc Suppl.) **26**, 459 (1992).

[45] M.S. Alam *et al.* (CLEO), Phys. Rev. **D50**, 43 (1994).

[46] M. Battle *et al.* (CLEO), Phys. Rev. Lett. **71**, 3922 (1993).

[47] R. Ammar *et al.* (CLEO), Phys. Rev. Lett. **71**, 674 (1993).

[48] B. Barish *et al.* (CLEO), CLEO Conference paper CLEO CONF 94-1 (1994).

[49] P. Frabetti *et al.* (E-687), Phys. Rev. Lett. **72**, 827 (1993) for the D_s^+; Phys. Lett. **B323**, 459 (1994) for the D^+ and D^0.

[50] J. Raab *et al.* (E-691), Phys. Rev. **D37**, 2391 (1988).

[51] D. Akerib *et al.* (CLEO), Phys. Rev. Lett. **71**, 3070 (1993).

[52] H. Albrecht *et al.* (ARGUS), DESY preprint DESY-94-094.

[53] J. Adler *et al.* (Mark III), Phys. Rev. Lett. **60**, 89 (1988).

[54] J.C. Anjos *et al.* (E-691), Phys. Rev. Lett. **60**, 1239 (1988).

[55] D. Cinabro *et al.* (CLEO), Cornell preprint CLNS-93-1262 (1993).

[56] A. Bean *et al.* (CLEO), Phys. Rev. Lett. **71**, 647 (1993).

[57] J.C. Anjos *et al.* (E-691), Phys. Rev. Lett. **62**, 1587 (1989).

[58] G. Crawford *et al.* (CLEO), Phys. Rev. **D44**, 3394 (1991).

[59] P.L. Frabetti *et al.* (E687), Phys. Lett. **B315**, 203 (1993).

[60] P.L. Frabetti *et al.* (E-687), Phys. Lett. **B307**, 262 (1993).

[61] J.C. Anjos *et al.* (E-691), Phys. Rev. Lett. **62**, 722 (1989); **65**, 2630 (1990).

[62] K. Kodama *et al.* (E-653), Phys. Lett. **B286**, 187 (1992).

[63] H. Albrecht *et al.* (ARGUS), Phys. Lett. **B255**, 634 (1991).

[64] K. Kodama *et al.* (E-653), Phys. Lett. **B274**, 246 (1992).

[65] M. Wirbel *et al.*, Z. Phys. **C29**, 627 (1985).

[66] J.G. Körner and G.A. Schuler, Z. Phys. **C38**, 511 (1988).

[67] T. Altomari and L. Wolfenstein, Phys. Rev. **D37**, 681 (1988); F.J. Gilman and R.L. Singleton, Phys. Rev. **D41**, 142 (1990).

[68] C.W.Bernard, A.X. El-Khadra, and A. Soni, Phys. Rev. **D47**, 998 (1993).

[69] V. Lubicz *et al.*, Phys. Lett. **B274**, 415 (1992).

[70] P. Ball, V.M. Braun, and H.G. Dosch, Phys. Rev. **D44**, 3567 (1991).

[71] R. Baltrusaitis *et al.* (Mark III), Phys. Rev. Lett. **54**, 1978 (1985).

[72] K. Kodama *et al.* (E-653), Phys. Lett. **B313**, 260 (1993).

[73] C.W. Bernard, J.N. Labrenz, and A. Soni, Washington U. preprint UW-PT-93-06, (1993). Phys. Rev. **D47**, 998 (1993).

[74] A. Abada *et al.*, Nucl. Phys. **B376**, 172 (1992); G. Martinelli, talk at the Heavy Flavor Symposium, Montreal (1993).

[75] J. Adler *et al.* (Mark III), Phys. Rev. Lett. **60**, 1375 (1988).

[76] S. Aoki *et al.* (WA-75), Prog. Theor. Phys. **89** , 131 (1993).

[77] D. Acosta *et al.* (CLEO), Phys. Rev.**D49**, 5690 (1994).

[78] N. Isgur and M.B. Wise, Phys. Rev. Lett. **66**, 1130 (1991).

[79] S. Godfrey and R. Kokoski, Phys. Rev. **D43**, 1679 (1991).

[80] P.L. Frabetti *et al.* (E687), Phys. Rev. Lett. **72**, 324 1994).

[81] Y. Kubota *et al.* (CLEO), Phys. Rev. Lett. **72**, 1972 (1994).

[82] N. Isgur and M.B. Wise, Phys. Rev. Lett. **66**, 1130 (1991).

[83] S. Godfrey and R. Kokoski, Phys. Rev. **D43**, 1679 (1991).

[84] P.L. Frabetti *et al.* (E687), Phys. Rev. Lett. **72**, 324 1994).

[85] Y. Kubota *et al.* (CLEO), Phys. Rev. Lett. **72**, 1972 (1994).

[86] M. Gronau and D. London, Phys. Rev. Lett. **65**, 3381 (1990).

[87] Y. Kubota *et al.*, Nucl. Inst. Meth. **A310**, 66(1992).

[88] BABAR Collaboration, Letter of Intent for the Study of CP Violation and Heavy Flavor Physics at PEP-II, SLAC report SLAC-443 (1994).

[89] BELLE Collaboration, Letter of Intent (1994).

[90] CLEO Collaboration, CLEO-III Design Report (1993) and The CLEO-III Project, Cornell Report CLNS-93-1265(1993).